S3M 5.1: a distributed cryospheric model with dry and wet snow, data assimilation, glacier mass balance, and debris-driven melt

Francesco Avanzi[1], Simone Gabellani[1], Fabio Delogu[1], Francesco Silvestro[1], Edoardo Cremonese[2], Umberto Morra di Cella[2, 1], Sara Ratto[3], and Hervé Stevenin[3]

[1]CIMA Research Foundation, Via Armando Magliotto 2, 17100 Savona, Italy

[2]Climate Change Unit, Environmental Protection Agency of Aosta Valley, Loc. La Maladière, 48-11020 Saint-Christophe, Italy

[3]Regione Autonoma Valle d'Aosta, Centro funzionale regionale, Via Promis 2/a, 11100 Aosta, Italy

Correspondence: Francesco Avanzi (francesco.avanzi@cimafoundation.org)

Abstract.

By shifting winter precipitation into summer freshet, the cryosphere supports life across the world. The sensitivity of this shifting mechanism to climate ~~, as well as~~ and the role played by the cryosphere in the Earth energy budget ~~, has~~ have motivated the development of a broad spectrum of predictive models. Such models ~~rarely combine a high degree of physical realism in both the~~ represent seasonal snow and glaciers with various complexities, and generally are not integrated with hydrologic models describing the fate of meltwater through the hydrologic budget. We present S3M v5.1, a spatially explicit and hydrology-oriented cryospheric model that successfully ~~reconstructs~~ simulates seasonal snow and glacier evolution through time and that can be natively coupled with distributed hydrologic models. Model physics include precipitation-phase partitioning, snow and glacier ~~energy and~~ mass balances, snow rheology and hydraulics, ~~and~~ a hybrid temperature-index and radiation-driven melt parametrization, and a data-assimilation protocol. Comparatively novel aspects of S3M ~~with respect to the existing literature~~ are an explicit representation of the spatial patterns of snow liquid-water content, ~~an hybrid approach to snowmelt that decouples the radiation- and temperature-driven contributions, the~~ the implementation of the Δh parametrization for distributed ice-thickness change, and the inclusion of a distributed debris-driven melt factor. Focusing on its operational implementation in the ~~Italian~~ north-western Italian Alps, we show that S3M provides robust predictions of the snow and glacier mass balances at multiple scales, thus delivering the necessary information to support real-world hydrologic operations. S3M is well suited for both operational flood forecasting and basic research, including future scenarios of the fate of the cryosphere and water supply in a warming climate. The model is open source, and the paper comprises an user manual as well as resources to prepare input data and set up computational environments and libraries.

1 Introduction

The cryosphere is a decisive driver of the Earth system (Barry, 2011; Beniston et al., 2018). Besides altering surface albedo and so concurring to the regulation of global temperature (Flanner et al., 2011), snow and glaciers accumulate winter precipitation and release it during the warm, ~~summer season~~spring and summer seasons, when demand by societies and ecosystem services is comparatively high (Barnett et al., 2005). This shift in water supply supports water, food, and energy security across climates (Viviroli et al., 2007), with key ~~implications for worldwide societies and ecosystem services~~ societal implications (Sturm et al., 2017). For example, snow represents up to 80% of annual water supply in the semi-arid, largely summer-dry western US (Bales et al., 2006; Serreze et al., 1999; Skiles et al., 2018), while 1.4+ billion people in Asia rely on discharge from high-mountain, cryosphere-dominated regions (Immerzeel et al., 2010). Meanwhile, the Andean cryosphere ~~represents~~ acts as a significant freshwater resource for semi-arid regions of South America (Masiokas et al., 2020), with an estimated contribution of up to 27% to dry-season water supply in La Paz, Bolivia (Soruco et al., 2015).

Seasonality between winter accumulation and summer melt (Barnett et al., 2005), compounded by equally complex but more short-term processes such as rain-on-snow (Rössler et al., 2014), challenges decision makers like water-resources or hydropower managers, who need early and diverse information about snow-glacier amount, distribution, and melt timing to make accurate decisions on water use, allocation, and storage (Georgakakos et al., 2004; Anghileri et al., 2016; Avanzi et al., 2018). This need has catalyzed the development of a ~~large portfolio~~ variety of models to predict snowmelt- and icemelt-driven discharge (DeWalle and Rango, 2011), to the extent that cryosphere modeling is a dominating topic of both basic and applied contemporary geosciences (Dozier et al., 2016). Application for cryosphere models are not limited to water-supply and flood forecasting, but include avalanche hazard forecasting (Bartelt and Lehning, 2002; Vionnet et al., 2012), land-surface and ~~so~~ weather modeling (Dutra et al., 2010; Wang et al., 2017), and snowmaking (Hanzer et al., 2020). The projected rise in future temperature and aridity ~~(IPCC, 2013)~~ (IPCC, 2021) further prioritizes robust predictions of cryospheric water resources, because shrinking glaciers and decreasing snow accumulation may endanger water supply and its predictability (Harrison and Bales, 2016) – especially during droughts (Huning and AghaKouchak, 2020).

Cryospheric models intersect hydrology with thermodynamics and rheology and as such present a bewildering variety in process representation. Regarding seasonal snow, options range from detailed, physics-based micro-scale models ~~like the Swiss SNOWPACK (Bartelt and Lehning, 2002)or the French~~ to intermediate-complexity, energy-balance models or simple one-layer, temperature-index models. Some examples of such models include SNOWPACK (Bartelt and Lehning, 2002), Crocus (Vionnet et al., 2012), ~~to intermediate-complexity, simplified-energy-balance models like the UEB model (Tarboton and Luce, 1996) and~~ SMAP (Niwano et al., 2012), UEB (Tarboton and Luce, 1996), SNOBAL (Marks et al., 1998), ~~or to simple one-layer, temperature-index models (Martinec, 1975; De Michele et al., 2013; Avanzi et al., 2015)~~GEOtop (Zanotti et al., 2004; Rigon et al., 2006; E , the Factorial Snowpack Model (Essery, 2015), SRM (Martinec, 1975), or HyS (De Michele et al., 2013; Avanzi et al., 2015), among many others. From a glacier standpoint, the most recurring distinction resides around glacier movement being captured through complex ice-flow approaches, glacier-specific parametrizations of changes in thickness (Huss et al., 2010), an equilibrium relationship between glacier area and long-term climate (Schaefli et al., 2007), or non-dynamic mass balance (Bongio et al., 2016). Parametrizing melt beneath supraglacial debris is another frequent aspect of modeling discretion (Fyffe et al., 2014).

While detail in process representation may appear as the prime driver of model selection, in hydrologic practice this choice also depends on other four pragmatic factors, which make hydrology-oriented cryospheric models essentially different from those oriented to, e.g., avalanche hazard forecasting. First, streamflow generation in cold regions involves not only snow and glacier ice, but also precipitation-topography interactions (Blanchet et al., 2009; Mott et al., 2014; Cui et al., 2020), vegetation-water feedback mechanisms (Zheng et al., 2016; Avanzi et al., 2020), and soil-water storage (Bales et al., 2011). Thus, snow-ice hydrology is inherently spatially distributed and multi-scale (Dozier et al., 2016), with the focus being arguably more on distributed ~~and~~ than on point predictions (Blöschl, 1999). Second, high-elevation cryospheric regions remain largely ungauged (Rasmussen et al., 2012; Avanzi et al., 2021), meaning that the necessary input data to run complex models is ~~sparse~~often missing or sparse at best. This condition has favored parsimonious models (Bartolini et al., 2011) and data-assimilation schemes to remedy model deficiencies with independently observed data (Andreadis and Lettenmaier, 2006; Piazzi et al., 2018). Coupled with data sparsity is the third factor, that is, the evidence that simplified and complex models often yield comparable predictive accuracy for bulk processes relevant to the seasonal freshet, such as Snow and Ice Water Equivalent ~~(see DeWalle and Rango, 2011, for a definition), surface melt, and runoff~~ (Huss et al., 2010; Avanzi et al., 2016; Magnusson et al., 2015). This explains why hydrology-oriented cryospheric models tend to have low complexity when it comes to internal layering and micro-scale properties. Fourth, processes relevant to cryosphere water resources span horizons from a few hours (such as rain-on-snow events, see Würzer et al., 2017) to decades (such as glacier dynamics, see Huss et al., 2010), implying that models used for real-world forecasting must be efficient enough to provide landscape-scale predictions in a timely manner (say, a few hours, see Pagano et al., 2014). Ultimately, these four factors trace back to empiricism rather than reductionism being the dominant (and perhaps most successful) paradigm in hydrology (Savenije, 2009), owing to unresolved issues related to upscaling mechanicistic laws to the landscape and measuring the complete heterogeneity of hydrologic processes (Blöschl and Sivapalan, 1995; Beven, 2006).

Here, we present Snow Multidata Mapping and Modeling (S3M) v5.1, a snow and glacier model developed ~~and maintained~~ by CIMA Research Foundation (https://www.cimafoundation.org/). ~~S3M fulfills all the four factors of hydrology-oriented cryospheric models outlined above, including being spatially distributed, parsimonious as for both input-data requirements and complexity, and enough computationally efficient to be deployed in operational, real-time flood-forecasting chains (Laiolo et al., 2014) .~~ Specific aspects of interest in S3M are (1) a spatially explicit prediction of both dry and wet-snow spatial patterns~~and so~~ , as well as bulk snowpack liquid water content (θ_W, in vol%), an increasingly decisive variable for snowmelt and avalanche ~~forecasting (Techel and Pielmeier, 2011; Wever et al., 2014; Avanzi et al., 2015; Wever et al., 2016)~~hazard forecasting (Techel and Pielmei ; (2) the combination of both snow and glacier mass dynamics in a coherent modeling framework, including the so-called Δh parametrization by Huss et al. (2010) and melt beneath supraglacial debris; (3) provisions for assimilating various decision-relevant variables like SWE, snow depth, and satellite-based snow-cover area. S3M v5.1 is the last generation of a model originally proposed by Boni et al. (2010), but significantly developed thereafter (henceforth, simply S3M).

The paper is organized as follows: Section 2 focuses on model description, including both snow and glaciers. Section 3 presents an example of results for an inner alpine valley in north-western Italy where various versions of this model have been operational since the ~~early~~ 2000s (Aosta valley). Finally, sections 4 discusses model applicability and future developments. The ~~Appendix~~ Supporting Information includes an User Manual discussing run preparation, execution, and post-processing.

2 Model description

The main modeling philosophy behind S3M is ~~a~~ to provide a ready-to-use tool for applications over large areas and when a short turnaround is needed. Thus, S3M complies with the four pragmatic factors of operational, hydrology-oriented cryospheric models outlined in the Introduction, including being spatially distributed, parsimonious as for both input-data requirements and complexity, and enough computationally efficient to be deployed in operational, real-time flood-forecasting chains (Laiolo et al., 2014) . These chains generally ingest an ensemble of weather predictions, may include parameter and/or state perturbation, assimilate remote-sensed and in-situ measurements, and must provide predictions for a variety of closure sections across the landscape in a matter of hours, if not minutes (Pagano et al., 2014). As such, they tend to be much more conceptual and computationally simple than research-oriented Earth-system models (Pagano et al., 2014). S3M tries to bridge the gap between these two realms, by accompanying simplicity and computational efficiency with an open-source environment that allows for frequent updates and improvements.

Parsimony implies a number of trade-off choices regarding what process representation to include, and to which extra cost. Current model physics include precipitation-phase partitioning, snow and glacier mass balances, a hybrid temperature-index and radiation-driven melt parametrization, snow rheology and hydraulics, and a data-assimilation protocol. Relevant drivers of snowpack and glacier evolution that are not yet included comprise internal snowpack energetics and the full energy balance, longwave losses, turbulent heat fluxes, sublimation, and canopy-snow interactions. While recent literature has showed that the added value of complex, physics-based snow models over more parsimonious alternatives *for variables that are relevant to hydrology* may sometimes be elusive (Rutter et al., 2009; Magnusson et al., 2015; Zaramella et al., 2019; Girons Lopez et al., 2020; Günth , designing more holistic and physics-based operational models remains a key to achieving the most accurate representation of snow temporal dynamics and spatial patterns, especially at fine resolutions (see for example results in Lafaysse et al., 2017; Vionnet et al., 2 . Strategies to include these processes in future releseases of S3M are discussed in Section 4.

S3M is a raster-based model, with the same set of equations being solved for each cell and no ~~spatial interdependency~~ lateral mass or energy transfer besides glacier change in thickness. A planned future release will include interdependency in the form of wind redistribution and melt routing through the snowpack (see Section 4). ~~The time step of the model is flexible, but it is generally set to 1 hour.~~ All input, state, and output variables are *distributed*, meaning they are passed to the model as rasters with fixed resolution in geographic degrees (see the ~~Appendix~~Supporting Information). All equations are ordinary differential equations with no need for iterative computations, so they are solved for all pixels in the simulation domain using a forward-Euler method~~.~~, as this method provides comparatively high numerical stability and minimizes computational time. The time step of the model is flexible, but it is generally set to 1 hour.

2.1 Definitions

We define snow and glacier ice as a mixture of three constituents: ice, liquid water, and air. Following De Michele et al. (2013) and Avanzi et al. (2015), the control volume of unitary area (h_{TOT}) for each pixel of the simulation domain is defined as:

$$h_{TOT} = h_G + h_S = \frac{V_{tot}}{A} \quad (1)$$

where h_G is glacier thickness (m), h_S is the height of snow (often referred to as snow depth, m), V_{tot} is the control volume in m^3 and A is the area of the pixel (m^2); $h_G = V_G/A$ and $h_S = V_S/A$, where V_G and V_S are the total volume of glacier and snow within the pixel under study. We define M_S and M_G as the mass of seasonal snow and glacier ice for each pixel, respectively (in kg). As for seasonal snow, this mass is $M_S = M_D + M_W$, with M_D and M_W the mass of the dry (snow grains) and wet (interstitial liquid water) constituents, respectively. The mass of air is assumed to be negligible compared to M_D and M_W (De Michele et al., 2013).

Snow is a foam of ice (Kirchner et al., 2001), meaning that the dry constituent occupies a porous skeleton of height h_D (m, volume V_D) and porosity $n = h_P/h_D$ (-), where h_P is the height of pores in the mixture (m, volume V_P). Thus, we define the density of the solid skeleton ρ_D (in kg m^{-3}) as:

$$\rho_D = \frac{M_D}{V_D} = \frac{\rho_i(V_D - V_P)}{V_D} = \rho_i(1-n), \quad (2)$$

where $\rho_i = 917$ kg m^{-3} is ice density. The density of the wet constituent is equal to that of liquid water: $\rho_W = M_W/V_W = 1000$ kg m^{-3} (V_W is the volume of liquid water in the mixture, height h_W). The density of glacier ice is assumed equal to ρ_i, with no progressive compression and/or air expulsion from cavities (Paterson, 1994).

During most of the snow season, the dry and wet constituents of the snowpack are both contained in h_D, the prevalent volume. However, an oversaturation condition takes place during the last instants of the snow season due to phase change (De Michele et al., 2013). Despite being a limit, virtually unmeasureable scenario, including this oversaturation condition is important from a numerical-stability standpoint. Thus, the total control volume of snow h_S (that is, snow depth) is hereby defined as:

$$h_S = h_D + \langle h_W - n h_D \rangle, \quad (3)$$

where $\langle\rangle$ are Macaulay brackets, which provide the argument if this is positive, otherwise 0. In other words, h_S is equal to the height of the porous structure h_D plus – if present – the oversaturated volume $\langle h_W - n h_D \rangle$ (De Michele et al., 2013). Accordingly, the bulk snow density ρ_S (in kg m^{-3}) is

$$\rho_S = \frac{M_D + M_W}{V_S} = \frac{\rho_D V_D + \rho_W V_W}{V_S} = \frac{\rho_D h_D + \rho_W h_W}{h_S} \quad (4)$$

and Snow Water Equivalent (in m w.e.) is $SWE = \rho_S \times h_S \times \rho_W^{-1}$. We also define the bulk volumetric liquid water content of the snowpack as:

$$\theta_W = \frac{V_W}{V_S} = \frac{h_W}{h_S}. \tag{5}$$

Glaciers are modeled as a single-phase material, the mass of liquid water and air being being negligible compared to glacier ice. Thus, the Ice Water Equivalent for glaciers (IWE) is:

$$IWE = \frac{\rho_i h_G}{\rho_W}. \tag{6}$$

Figure 1 summarizes the ~~main definitions, state variables , and inputs~~ prognostic variables and main mass fluxes of S3M. Dynamic inputs for S3M are total precipitation, air temperature, relative humidity, and incoming shortwave radiation (see the Supporting Information for details).

2.2 Snow: mass-conservation equations

The mass-conservation equations for the dry and wet constituents of the snowpack read as follows:

$$\frac{dM_D}{dt} = \hat{S}_f - \hat{M} + \hat{R} \tag{7}$$

$$\frac{dM_W}{dt} = \hat{R}_f + \hat{M} - \hat{R} - \hat{O}, \tag{8}$$

where $\hat{S}_f$ is the snowfall mass flux, $\hat{M}$ is the snowmelt mass flux, $\hat{R}$ is the refreezing mass flux, $\hat{R}_f$ is the rainfall mass flux, and $\hat{O}$ is the outflow mass flux (also known as snowpack runoff, see Avanzi et al., 2019). All these mass fluxes are expressed in kg Δt^{-1} and are denoted with a , as opposed to customary hydrologic fluxes in mm Δt^{-1}, which will be denoted without ˆ in the following. Given that $M_D = \rho_D h_D A$, we simplify Equation 7 as

$$\frac{1}{\rho_W A}\frac{d(\rho_D h_D A)}{dt} = \frac{\hat{S}_f - \hat{M} + \hat{R}}{\rho_W A} \tag{9}$$

to obtain

$$\frac{d}{dt}\left(\frac{\rho_D h_D}{\rho_W}\right) = \frac{dSWE_D}{dt} = S_f - M + R, \tag{10}$$

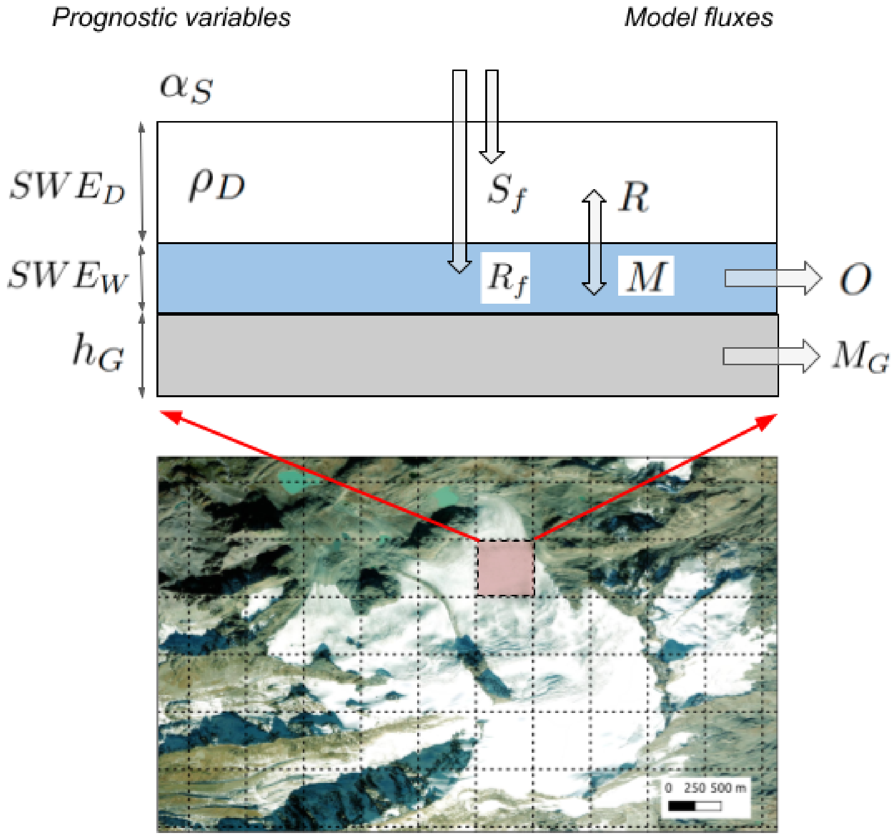

Figure 1. ~~Main definitions, state~~ Prognostic variables ~~,~~ and ~~inputs~~ main mass fluxes of S3M (see Section 2 for details). ~~P is total precipitation, T_{air} is air temperature,~~ α_S is snow albedo (-), ~~S_r is incoming shortwave radiation,~~ S_f and R_f are snowfall and rainfall rate (mm Δt^{-1}), respectively, ~~RH is relative humidity,~~ SWE_D (mm) and ρ_D (kg m^{-3}) are dry Snow Water Equivalent and dry bulk snow density, respectively, SWE_W ~~and θ_W are~~ is wet Snow Water Equivalent ~~and bulk volumetric liquid water content~~(mm), R, M, and O are snow refreezing, melt, and outflow, respectively (mm Δt^{-1}), h_G is glacier thickness (m), ~~f_{debris}~~ M_G is ~~a coefficient accounting~~ ice melt (mm Δt^{-1}). Note that albedo is here listed as prognostic variable for clarity, but the ~~modulating effect of thick debris on ice melting~~actual, ~~M_G~~ underlying prognostic variable is ~~ice melt~~technically snow age A_s. The background image is Rutor glacier in north-western Italy.

where SWE_D is the dry-snow water equivalent ($\rho_D h_D \rho_W^{-1}$) and S_f, M, and R are the snowfall, snowmelt, and refreezing mass fluxes in mm w.e. Δt^{-1}. Note that SWE_D and all related mass fluxes will henceforth be expressed in mm w.e., with a conversion by 1000 mm m^{-1} being implicitly included between Equation 7 and 10. Likewise, we simplify Equation 8 as

$$\frac{1}{\rho_W A}\frac{d(\rho_W h_W A)}{dt} = \frac{\hat{R}_f + \hat{M} - \hat{R} - \hat{O}}{\rho_W A} \tag{11}$$

to obtain

$$\frac{dSWE_W}{dt} = R_f + M - R - O, \tag{12}$$

with SWE_W being the wet-snow water equivalent, and R_f and O being the rainfall and snowpack-runoff mass flux in mm w.e (again, note that SWE_W and all related mass fluxes will henceforth be expressed in mm w.e., with a conversion by 1000 mm m^{-1} being implicitly included between Equation 8 and 12).

Equations 10 and 12 are the two fundamental snow mass-conservation equations of S3M, which thus offers a spatially explicit, prognostic simulation of both the dry and wet constituents of snow (total SWE being instead a diagnostic variable: $SWE = SWE_D + SWE_W$) . This phase separation follows De Michele et al. (2013) and Avanzi et al. (2015), with two differences. First, equations in De Michele et al. (2013) and Avanzi et al. (2015) were written using h_D and h_W as main state variables, whereas here we used SWE_D and SWE_W, which allows a more compact formulation of mass-conservation equations since no density-compaction term is necessary in Equation 10. Second, Avanzi et al. (2015) introduced a mass-conservation equation for a third constituent, refrozen ice. Here, we directly included the refreezing term in Equations 10 and 12.

S3M assumes that simulated SWE, as well as all other model variables and fluxes, are representative of spatially averaged snowpack conditions across the simulated pixel. Whilst this assumption is coherent with current practice in many hydrologic models, it does not take advantage of scaling mechanisms with fractional snow-covered area. Adding fractional snow cover and a full reconstruction of sub-grid snow-depletion curves is an important direction of future development.

2.3 Snow: mass-flux parametrizations

Mass fluxes in Equations 10 and 12 requiring specific parametrizations are snowfall and rainfall (R_f and S_f), snowmelt and refreezing (M and R), and snowpack runoff (O).

2.3.1 Precipitation-phase partitioning

Snowfall and rainfall in S3M are estimated from total precipitation (P), an input for the model; precipitation-phase partitioning is based on the empirical approach described in Froidurot et al. (2014):

$$S_f = p_s P \tag{13a}$$

$$R_f = p_r P \tag{13b}$$

$$p_{\underline{f}s} = 1 - p_r \tag{13c}$$

$$p_r = \frac{1}{1 + e^{\alpha + \beta T_{air} + \gamma RH}}, \tag{13d}$$

where p_s and p_r are the probabilities of snowfall and rainfall, respectively, α, β, and γ are fixed parameters derived by Froidurot et al. (2014), T_{air} is air temperature in °C, and RH is relative humidity in %. S3M assumes p_s and p_r to be equal to the actual proportions of rainfall and snowfall over total precipitation. Following Froidurot et al. (2014) and references therein, $\alpha = 22$, $\beta = -2.7$, and $\gamma = -0.2$.

Fresh snow is assumed to be dry, with density ρ_f depending on air temperature (Pomeroy and Brun, 2001):

$$\rho_f = 67.9 + 51.25 e^{\frac{T_{air}}{2.59}}. \tag{14}$$

2.3.2 Snowmelt and refreezing

Snowmelt (M) is computed if *both* concurrent T_{air} *and* mean air-temperature over the previous 10 days ($\bar{T}_{10d}$) are greater than, or equal to, T_τ, a user-defined threshold usually assumed equal to 1 °C (Pellicciotti et al., 2005); otherwise, $M = 0$. The first condition is standard in degree-day models and accounts for snow melt occurring during periods with a supposedly positive energy balance (meaning a net gain of energy for the snowpack). The second condition is a novel addition of S3M to the literature to keep track of cold content using a pragmatic and parsimonious approach (cold content being a measure of the snowpack-energy deficit to be satisfied for actual melt to start, see Jennings et al., 2018). The basic idea is that $\bar{T}_{10d}$ evolves with a certain delay compared to T_{air}, so that setting an additional threshold on $\bar{T}_{10d}$ helps avoiding non-physical melt during short warm spells that come after a somewhat long cold period. Other simple approaches to estimate cold content exist, such as that based on mean-seasonal temperature by Schaefli and Huss (2011), but are all also in their early stages. Our approach is the result of intensive trial and error , and seems yielding and yields satisfactory results – especially in suppressing erroneous mid-winter melt episodes that do not appear in validation data.

Snowmelt is parametrized using a hybrid physics-based and degree-day approach decoupling radiative forcing from temperature-driven melt (similarly to Pellicciotti et al., 2005):

$$M = m_{rad} \left[\frac{(1-\alpha_S) S_r}{\rho_W \lambda_f} \right] \Delta t + c_M m_r (T_{air} - T_\tau), \tag{15}$$

where S_r is incoming shortwave radiation (an input for S3M, in W m^{-2}), α_S is snow broadband albedo (-) , λ_f is the specific latent heat of fusion (0.334 MJ kg^{-1}), m_r is a degree-day parameter (mm °C^{-1} day^{-1}) , m_{rad} is a an adimensional modulating factor to convert shortwave radiation into actual melt (similar to an efficiency parameter, see below), and c_M is a timestep-adjusting parameter.

S3M assumes S_r to be in W m^{-2}, T_{air} in °C, m_{rad} to be adimensional, and m_r in mm °C^{-1} day^{-1}. While S_r is internally converted to MJ m^{-2} according to model timestep (see Δt in Equation 15), the air-temperature part of Equation 15 is computed by first considering an equivalent day with average temperature equal to T_{air}, regardless of modelling time step. The snowmelt part depending on air temperature is then readjusted by $c_M = \Delta t / 86400$ to pass from one day to the actual time step (Δt is in seconds). This workaround is due to the degree-day approach being originally conceived for daily applications (see for instance Hock, 1999, 2003; De Michele et al., 2013, and references therein) (see Hock, 1999, 2003; De Michele et al., 2013, and . Note that S3M internally sets S_r to 0 between 7PM and 7AMaccording to forcing timestamps, while proper , in order to remove spurious noise in radiation sensors (this could be improved by computing time of local sunrise and sunset). Proper unit conversions are implicitly included in the radiation part of Equation 15 to first pass from J m^{-2} to MJ m^{-2} and then from m w.e. to mm w.e.

Broadband albedo is computed once per day at midnight (timestamp time) according to Laramie and Schaake (1972):

$$\alpha_S = 0.5 + 0.45 e^{-\tau_\alpha A_s}, \tag{16}$$

where τ_α is an albedo-decay coefficient equal to 0.12 d^{-1} if average air temperature over the previous 24 hours is higher than 0°Cand , and otherwise equal to 0.05 d^{-1}otherwise . A_s is snow age (in d), defined as the number of days since the last significant snowfall. S3M considers as significant snowfall one day with at least 3 mm of total snowfall. Snow age A_s is updated every day at midnight(timestamp time) : if cumulative snowfall during the previous 24 hours is less than 3 mm, then snow age is increased by 1 day; if not, than snow age is reset to 0.

Similarly to other snowmelt models (Rango and Martinec, 1995), melt parameters m_r (mm °C^{-1} d^{-1}) and m_{rad} (-) are calibration-based, although the sensitivity of S3M to both is rather low (see results in Section 3) . This low sensitivity is likely because explicitly separating the radiation- and temperature-driven components of melt brings these parameters closer to physics a fully first-principals energy balance model than standard degree-day approaches(see Section 3). Yet, this hybrid approach used by S3M has been rarely considered .

An explicit separation between the temperature- and the radiation-driven components has been underused in the literature. For example, the seminal work by Hock (1999) did include potential radiation, but embedded it into a degree-day parameter rather than explicitly separating the radiation and the temperature components. Follum et al. (2015) replaced the temperature term with a proxy from a radiation balance, which may be suitable in regions where snowmelt is mostly radiation driven (e.g., the western US, see Bales et al., 2006), but would need some form of temperature dependency in temperate regions like the Alps.

Pellicciotti et al. (2005) are among the few examples where the radiation and the temperature component are fully decoupled, but they focused on glacier ice during summer, which is an isothermal , very efficient condition . This isothermal condition is very efficient for shortwave radiation to convert into actual melt. However, applying the original approach by Pellicciotti et al. (2005) to snow revealed a tendency to overestimate melt rate early in the snowmelt season, because it assumes net shortwave radiation to translate into melt regardless of the actual cold content. In subfreezing conditions, in fact, a fraction of net shortwave radiation is used to raise snow temperature, a mechanism that becomes increasingly unimportant as the season progresses and snow conditions tend towards isothermal. To mimic this transition from subfreezing to isothermal conditions, we propose a modification to the original approach by Pellicciotti et al. (2005) in the form of a novel 10-day-temperature-modulated efficiency parameter m_{rad} that increases with $\bar{T}_{10d}$ according to a sigmoid function (Figure 2, a):

$$m_{rad} = 0.49338 \times \arctan(0.27439 \times \bar{T}_{10d} - 0.5988) - 0.49338 \times \frac{3.14}{2} + m'_{rad}. \tag{17}$$

While parameter m'_{rad} is user-defined, we note that $m'_{rad} \sim 1.10$ means that $m_{rad} \to 1$ when $\bar{T}_{10d} > 10$ °C. This corresponds to a 1:1 conversion of net shortwave radiation into melt when isothermal conditions like those by Pellicciotti et al. (2005) dominate. On the other hand, $m_{rad} \to 0$ when $\bar{T}_{10d} \to 0$ °C. m_{rad} is set to 0 if the equation above predicted predicts a negative value. Note that this temperature-modulated efficiency parameter is a proxy of cold content, but it does not imply an *explicit* computation of cold content. It is a first attempt to take into account thermal inertia in subfreezing conditions and how it is related to external climate, similarly to Schaefli and Huss (2011). At the present stage, no relation with snow depth or internal snow temperature is included, but this could be a fruitful addition.

S3M considers a similar relation between $\bar{T}_{10d}$ and m_r through a sigmoid function and a user-defined tuning parameter (m'_r, see Figure 2, b):

$$m_r = 0.598862 \times \arctan(0.27439 \times \bar{T}_{10d} - 0.5988) - 0.598862 \times \frac{3.14}{2} + m'_r. \tag{18}$$

Here again, we note that $m'_r \sim 1.40$ mm C^{-1} d^{-1} corresponds to ∼0.05 mm C^{-1} h^{-1} when $\bar{T}_{10d} > 10$ °C, which agrees with estimates by Pellicciotti et al. (2005) in isothermal conditions on ice. While establishing a relationship between melt parameters and $\bar{T}_{10d}$ is novel, note that previous literature has already suggested a seasonal variability in the degree-day parameter that is conceptually similar to our approach (see Bongio et al., 2016, and references therein). Also, note that m_r should be much smaller than degree-day parameters listed by Hock (2003), because the latter were supposed to account for both the temperature-driven and radiation-driven component of snowmelt. Parameter m_r is set to 0 in case the equation above returned a value lower than 0.

Refreezing (R) is computed when $T_{air} < T_\tau$, using a simple degree-day approach as in Avanzi et al. (2015):

$$R = -c_M m_r \left(T_{air} - T_\tau\right). \tag{19}$$

Compared to Differently from Avanzi et al. (2015) or Schaefli et al. (2014), we do not decrease m_r by a reduction factor when computing refreezing. In standard degree-day models that do not separate the temperature and radiation components of melt, that reduction factor conceptually accounts for refreezing melt rate being smaller than snowmelt rate for the same temperature difference, given the usual lack of incoming-shortwave radiation during refreezing-prone periods. This reduction factor is not necessary in S3M, because the contribution of incoming-shortwave radiation is explicitly accounted for in Equation 15 and excluded in Equation 19; in other words, m_r only accounts for turbulent and longwave-radiation factors.

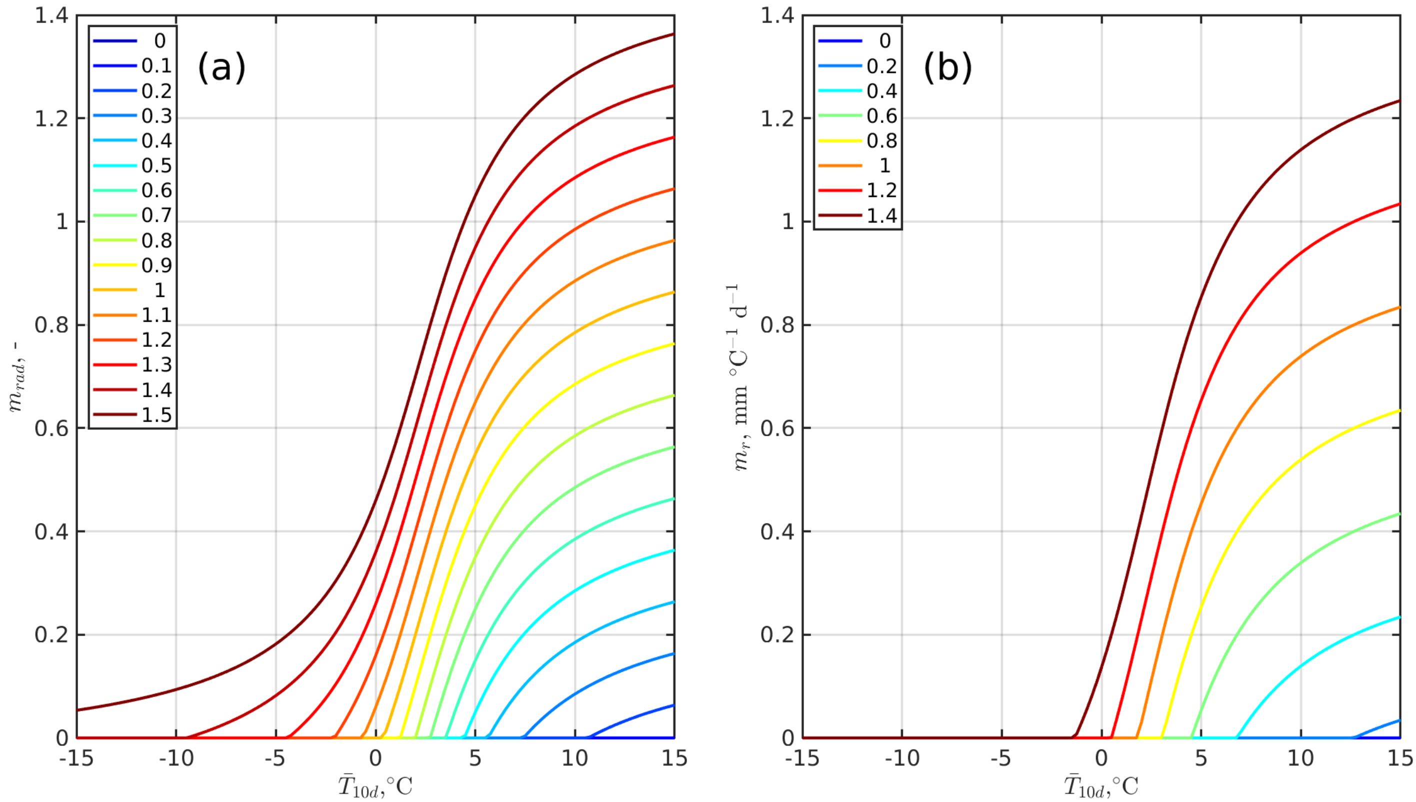

Figure 2. Values of the modulating parameter converting shortwave radiation into actual melt (m_{rad}, panel a) and the degree-day melt parameter (m_r, panel b) as a function of mean air-temperature over the previous 10 days ($\bar{T}_{10d}$) and various values of two tuning parameters (m'_{rad} and m'_r, see figure legends for values).

2.3.3 Snowpack runoff

While the term *runoff* in catchment hydrology generally denotes *overland flow*, we follow here customary nomenclature in snow hydrology and call snowpack runoff the amount of liquid water discharged by the snowpack (Wever et al., 2014). This flux is parametrized according to a matrix-flow approximation (Colbeck, 1972; Avanzi et al., 2015, 2016):

$$O = \alpha \frac{\rho_W g K_W}{\mu_W}, \tag{20}$$

where μ_W is water dynamic viscosity, g is acceleration due to gravity, K_W is the intrinsic permeability of water in snow (m^2), and α is a time- and unit-conversion parameter (equal to 1000 mm m$^{-1} \times \Delta t$, with Δt in seconds). Assuming $\rho_W = 1000$ kg m^{-3}, $g = 9.81$ m s^{-2}, and $\mu_W = 1.79 \times 10^{-2}$ kg m^{-1} s^{-1} (DeWalle and Rango, 2011), then

$$O = \alpha \alpha' K_W, \tag{21}$$

with $\alpha' = 5.47 \times 10^5$ m^{-1} s^{-1}. We predict K_W following again Colbeck (1972):

$$K_W = K S^{\star 3}, \tag{22}$$

where K is the intrinsic permeability of snow (in m^2) and $S^\star$ is the effective saturation degree:

$$S^\star = \frac{Sr - Sr_i}{1 - Sr_i}. \tag{23}$$

Sr_i is the irreducible saturation degree computed based on Kelleners et al. (2009) as $0.02\rho_D \rho_W^{-1} n^{-1}$, whereas $Sr = h_W n^{-1} h_D^{-1}$ is the saturation degree. Snowpack runoff is set to 0 if $Sr < Sr_i$.

Intrinsic permeability of snow is predicted based on Calonne et al. (2012):

$$K = 3 r_e^2 e^{-0.013\rho_D}, \tag{24}$$

where r_e is the equivalent sphere radius (m), a conceptual, characteristic length of snow microstructure corresponding "to the radius of a monodisperse collection of spheres having the same specific surface area (SSA) as the sample considered" (Calonne et al., 2012). Variable r_e or SSA (m^2 kg^{-1}) are likely the most objective metrics of snow microstructure to date (Carmagnola et al., 2014), traditional grain size being subjective and cumbersome to measure (Fierz et al., 2009). Still, SSA and r_e are insufficient to fully characterize snow structure, because grain shape also plays an important role in the two-point correlation function (Krol and Löwe, 2016). We relate r_e to SSA by definition:

$$r_e = \frac{3}{SSA \rho_i} \tag{25}$$

and diagnostically estimate SSA following Domine et al. (2007):

$$SSA' = -308.2 ln(\rho'_D) - 206, \tag{26}$$

with SSA' being SSA in cm^2 g^{-1} and ρ'_D is ρ_D in g cm^{-3}. We used Equation 26 to predict SSA because S3M currently does not include a prognostic simulation of snow microstructure. However, Domine et al. (2007) clearly show that density alone is a modest predictor of SSA ($R^2 = 0.43$). Future work will augment snow microphysics to better capture SSA seasonal patterns and how they relate to snow metamorphism (Legagneux et al., 2002; Domine et al., 2013; Carmagnola et al., 2014; Morin et al., 2013), especially in wet conditions (Avanzi et al., 2017; Hirashima et al., 2019).

Following Avanzi et al. (2015) In order to avoid high saturation values in a shallow snowpack to cause large outflow rates and non-physical negative values of SWE_W , Equation 20 is used as long as $Sr < 0.5$ or $SWE_D > 10$ mm w.e.. This is because Avanzi et al. (2015) report instabilities of Equation 20 for high saturation values or a very shallow snowpack. In situations with $Sr \geq 0.5$ or $SWE_D < 10$ mm, Equation 20 is thus bypassed and SWE_W is directly converted into snowpack runoff.

2.3.4 Dry-density equation

Differently from liquid water, bulk dry-snow density in S3M is not invariant with time because of three main factors: compaction, new-snow events, and refreezing:

$$\frac{d\rho_D}{dt} = \left.\frac{d\rho_D}{dt}\right|_{comp} + \left.\frac{d\rho_D}{dt}\right|_{snowf} + \left.\frac{d\rho_D}{dt}\right|_{ref}. \tag{27}$$

These factors do not include snow metamorphisms (Pinzer, 2009), mainly because of the scale mismatch between such processes and the one-layer approach of S3M.

Regarding compaction, we assume a linear profile for stress with depth and start from the momentum-conservation equation for a representative element at 66% depth, which experiences an average stress :

$$\sigma_v = 0.66\rho_D g h_D = 0.66 SWE_D \rho_W g, \tag{28}$$

with σ_v being vertical stress. Equation 28 is then coupled with a viscous rheological equation to obtain, via the definition of the vertical strain rate:

$$\left.\frac{d\rho_D}{dt}\right|_{comp} = \rho_D \frac{\sigma_v}{\eta} = \rho_D \frac{0.66 SWE_D \rho_W g}{\eta}, \tag{29}$$

with η being viscosity. We finally follow De Michele et al. (2013) and reference references therein and define viscosity as an exponential function of dry-snow density and snow temperature:

$$\left.\frac{d\rho_D}{dt}\right|_{comp} = 0.66 c_{\Delta t} c_1 \rho_D SWE_D \rho_W e^{0.08 T_S - 0.021\rho_D}, \tag{30}$$

or in a more compact form as:

$$\left.\frac{d\rho_D}{dt}\right|_{comp} = 0.66 c_{\Delta t} c_1 \rho_D^2 h_D e^{0.08 T_S - 0.021\rho_D}. \tag{31}$$

T_S is snow mean temperature (°C), $c_1 = 0.001$ m^2 h^{-1} kg^{-1}, and $c_{\Delta t}$ is a timestep-adjusting coefficient ($\Delta t \times 3600^{-1}$ s^{-1} h, with Δt in seconds).

Because S3M does not solve for the full energy balance, it also does not simulate snow-temperature profiles. If The fact that snow temperature in S3M has no implication for snow melt, compounded by the sensitivity of the settling equation to snow temperature being rather small (not reported for brevity) led us to introduce a simple parametrization here: if $T_{air} < 0$°C, snow mean temperature is assumed to follow a linear profile between snow-surface temperature and ground surface (assumed equal to T_{air} and 0 °C, respectively, see Ohara and Kavvas, 2006), while (assumed equal to T_{air} and 0 °C, respectively, followi , while otherwise it is set to 0°Cotherwise .

New events change bulk-snow density proportionally to snowfall depth versus existing-snow depth:

$$\rho_D(t + \Delta t) = \frac{SWE_D + S_f}{\left(\frac{S_f}{\rho_f} + \frac{SWE_D}{\rho_D}\right)}. \tag{32}$$

We handle refreezing with a similar approach to new events, thus implying that refreezing has no impact on snow structure besides the associated volume expansion from liquid water to ice: :

$$\rho_D(t + \Delta_t) = \frac{SWE_D + R}{\left(\frac{R}{\rho_i} + \frac{SWE_D}{\rho_D}\right)}. \tag{33}$$

This assumption has been discussed previously, with mixed results (Gallet et al., 2014; Avanzi et al., 2017).

2.3.5 Data assimilation

The assimilation framework of S3M is a result of CIMA's operational-forecasting procedures as summarized into the Flood-PROOFS suite (Laiolo et al., 2014; Avanzi et al., 2021). These procedures – external to S3M – include generating maps of snow depth and satellite-based scene classification (hence, snow-covered area – SCA), as well as processing SWE maps from third parties (e.g., from interpolation of ground manual measurements, see Avanzi et al., 2021). Given that snow depth and satellite maps are generated with a comparatively high frequency (up to daily), their assimilation in S3M is performed in correspondence to the timestamp to which they refer (this nominal timestamps must be the same for both snow-depth and satellite maps, collectively referred to as Updating maps). SWE maps have various temporal frequencies (usually, weekly), thus S3M allows the user to specify a temporal window of influence, that is, a period after the official issue date of the SWE map during which the map is assumed to be valid.

Assimilation of Updating maps also additionally requires a Kernel map and a Quality map. The Kernel (K) is generally an output of the geostatistics-based interpolation method used employed to generate the snow-depth maps and is used to optimally combine observations and model predictions (see below). Instead, the Quality map is used to automatically skip assimilation when values in this map are below an user-defined threshold. For example, the operational convention in Flood-PROOFS is to forego assimilation during days with large cloud obstruction. Thus, in Flood-PROOFS the Quality map for a given day is computed as the ratio between pixels classified as snow or ground over the total number of pixels (so, in fact, this map reports the same scalar for each pixel). In this way, quality is a measure of the proportion of the satellite map that is covered by clouds. We stress, however, that this quality can be defined based on any user's need, with S3M skipping assimilation below a quality threshold even if the corresponding snow-depth map was available.

Prior to assimilation, S3M blends information from the snow depth and the SCA maps based on quality. For example, K is doubled wherever quality is 2.5 times the quality threshold and the satellite indicates ground (ID = 0). Also, snow-depth maps are set to 0 wherever quality is greater than the quality threshold and the satellite indicates ground. Finally, snow-depth maps are set to missing values wherever quality is lower than the quality threshold, modeled SWE is less than 20 mm w.e., and the satellite indicates clouds, no decision, or no data (ID = 2, 3, and -1, respectively).

SWE maps, on the other hand, use neither a quality flag nor a spatially distributed Kernel, again owing to how these maps are received and handled by Flood-PROOFS. For assimilating SWE maps, K is thus assumed to be a function of time elapsed since the issue date, with no spatial variability:

$$K = We^{\frac{-(t'-t_{SWE})^2}{0.5\sigma^2}}, \tag{34}$$

where t_{SWE} is the official issue time of the SWE map, t' is time relative to this issue date (in days), and σ is equal to half of the validity days after SWE-map issue date (user-defined parameter, see the Appendix Supporting Information). On the same date of the issue date, $t' = t_{SWE}$ and so $K = W$, where W is a user-assigned maximum weight of the map to be assimilated. No quality threshold is used for SWE maps given that they are usually the result of reanalysis rather than real-time automatic processing.

Currently, S3M performs data-assimilation exclusively in the form of SWE. Thus, snow-depth-map assimilation requires a preliminary step to convert snow depth into SWE via modeled bulk-snow density:

$$SWE_{obs} = \frac{h_{S,obs} \times \rho_{S,S3M}}{\rho_W}, \tag{35}$$

where $h_{S,obs}$ and $\rho_{S,S3M}$ are observed snow depth according to the snow-depth map and simulated bulk-snow density according to S3M, respectively. This step implicitly assumes that snow density is a less relevant source of uncertainty than snow depth in estimating SWE, which is supported by snow-density temporal patterns being consistent from year to year (Mizukami and Perica, 2008).

Updating and SWE maps are assimilated into S3M using a Newtonian-relaxation approach:

$$SWE_{S3M,post} = SWE_{S3M,prior} + K\left(SWE_{obs} - SWE_{S3M,prior}\right), \tag{36}$$

where $SWE_{S3M,post}$ and $SWE_{S3M,prior}$ are the a-posteriori and a-priori SWE. Note that Newtonian Relaxation (also known as nudging) is different from direct insertion, where model estimates are directly replaced by observations; in a nudging scheme, the correction factor is proportional to the difference between observations and model outputs via a Kernel weight (Boni et al., 2010; Mazzoleni et al., 2018).

After assimilating bulk SWE, a few state prognostic variables of S3M are modified through factor U_{SWE}:

$$U_{SWE} = \frac{SWE_{S3M,post}}{SWE_{S3M,prior}} \tag{37}$$

$$SWE_{D,S3M,post} = U_{SWE} \times SWE_{D,S3M,prior} \tag{38}$$

$$SWE_{W,S3M,post} = U_{SWE} \times SWE_{W,S3M,prior}. \tag{39}$$

This step is needed since total SWE in S3M v5.1 is only a diagnostic variable, and assimilating it does not affect model predictions unless the true prognostic variables are also modified (in this case, SWE_D and SWE_W). Factor U_{SWE} assumes that both the dry and the wet phases are proportionally affected by data assimilation. It is also assumed that dry-snow density does not change during assimilation. Given that dry-density evolution does depend on SWE_D, this is a simplification.

S3M also optionally supports assimilating only positive differences in Equation 36, that is, only correcting modeled SWE if observations are larger than simulations. This experimental configuration may help helps when assimilating observed SWE mainly aims at correcting for precipitation under-catch , while the user would like the ablation season to be unaffected by assimilation. (Ryan et al., 2008). Such an approach is, e.g., standard in avalanche-forecasting models like SNOWPACK (Lehning et al., 2002). Note, however, that However, this experimental configuration will likely override the SCA component of the assimilation package, because SCA assimilation in S3M is performed indirectly via setting observed snow depth to zero in areas with observed ground.

The last step in the snow component is to perform a set of sanity checks (e.g., set to zero all state variables where SWE$\rightarrow 0$) and to compute the snow mask, a binary map with the same size of the simulation domain reporting 1 where $SWE > 0.1$ mm, and 0 elsewhere. This mask is an important output of S3M that is sometimes used by hydrologic models to adjust process representation in areas of snow (for example, inhibiting evapotranspiration).

2.4 Glacier component

The glacier component of S3M offers three alternative modules: (1) a simple, melt-only approach with no mass balance and no snow-to-ice conversion ; this approach (G1), which is usually the default choice for short-term flood-forecasting-oriented simulations; (2) a melt-only approach with mass balance but no parametrization of glacier dynamics or and no snow-to-ice conversion (G2) ; (3) an approach with a full mass balance, a parametrization of glacier dynamics (the Δh parametrization), and snow-to-ice conversion (G3) . The last two approaches are the most suited options for long-term, climate-scenario-oriented simulations.

2.4.1 G1: Melt-only approach, no mass balance, no glacier dynamics, no snow-to-ice conversion

In the most basic approach (G1) , glacier melt takes place on snow-free glacier pixels with a similar parametrization as that of snow (Equation 15), with only two changes. The first is that glacier albedo α_G is constant (0.4, see Davaze et al., 2018), as opposed to snow albedo changing with snow age. The second change is that ice-melt rate (M_G) on debris-covered glaciers may be corrected compared to the theoretical melt rate on debris-free glaciers ($M_G^\star$) using a multiplicative reduction factor, f_{debris} (Huss and Fischer, 2016):

$$M_G = (1 - f_{debris})M_G^\star. \tag{40}$$

The correction factor f_{debris} can be estimated with various approaches, for example following Huss and Fischer (2016) who prescribed it based on the so-called Østrem curve. Accordingly, values of f_{debris} are generally smaller than 0 for very shallow debris (up to ∼5 cm), and between 0 and 1 otherwise (Nicholson and Benn, 2006). S3M expects f_{debris} to be a spatially distributed, input parameter included in the so-called static-data suite (see Section ?? the Supporting Information). Glacier melt is directly converted into ice runoff, with no routing (Figure 1). Glacier pixels are defined based on a glacier mask (see Section ?? the Supporting Information).

2.5 G2: Melt-only approach , with mass balance, no glacier dynamics, no snow-to-ice conversion

This approach (G2) is equivalent to G1 with the only difference that glacier thickness (h_G) is dynamically updated every hour based on glacier melt. To do so, ice melt in mm w.e. according to Equation 15 and optionally Equation 40 is converted to meters of ice using ice density ρ_i. The mass-conservation equation reads:

$$\frac{dIWE}{dt} = -M_G. \tag{41}$$

Wherever $h_G \to 0$ as a result of multi-year melt, ice melt on that pixel is not computed anymore. S3M expects h_G to be a spatially distributed input (included either in the so-called restart data or in the static data, see Section ?? the Supporting Information).

2.6 G3: Full mass-balance approach with glacier dynamics and snow-to-ice conversion

This approach – G3, ideal for multi-year simulations – includes snow-to-ice conversion and a specific mass-redistribution approach called the Δh parametrization (Huss et al., 2010), which allows one to implicitly account for glacier-movement effects without implementing a full ice-flow model. Because the Δh parametrization is better suited for multi-year time scales rather than day-to-day thickness changes, module G3 requires the user to define the month of water-year start, so that S3M will accumulate glacier melt for each pixel throughout the water year and update h_G at the beginning of each new water year. Regardless of this accumulation procedure, ice melt is still outputed every time step, so that seasonality in runoff-generation processes is preserved. In other words, this accumulation procedure only regards changes in glacier thickness and not ice-runoff generation. This is important in case S3M was coupled with a hydrologic model.

Snow-to-ice conversion is performed by simply prescribing that, on pixels with $h_G > 0$, any residual SWE at the end of each water year is added to h_G. Consequently, SWE as well as all snow-related bulk state variables are reset to 0. This pragmatic approach reset is not performed in areas where SWE> 0 and $h_G = 0$ at the end of the season; in such conditions, the snowpack is maintained through the start of the new water year. This approach is less rigorous than considering firn, the intermediate step between snow and ice. While previous work by Schaefli et al. (2005) in Switzerland showed that the use of a separate degree day factor for firn may not significantly improve hydrologic predictions, including firn remains an important step of future work (see Section 4).

As for the Δh parametrization, this is presented in Huss et al. (2010) and further discussed for hydrologic models by Seibert et al. (2018), so we limit ourselves to a short overview here. This approach starts from the empirical intuition that glacier-thickness changes as a result of both the mass balance and glacier flow have recurring patterns throughout seasons of persistently negative mass balances (Huss et al., 2010). By parametrizing parameterizing these recurring patterns, the Δh parametrization allows one to simulate the effect of movement in addition to the mass balance without a complex ice-flow model. These patterns are derived through differentiating two digital surface models (Huss et al., 2010) and then fitting a glacier-specific power law like

$$\Delta h = (h_r + a)^{\gamma} + b(h_r + a) + c, \tag{42}$$

where a, γ, b, c are calibration parameters, Δh is the change in surface elevation (normalized by the maximum decrease across all glacier pixels), and h_r is normalized glacier elevation defined as

$$h_r = \frac{h_{max} - h}{h_{max} - h_{min}}, \tag{43}$$

with h_{max} and h_{min} being the maximum and minimum elevations of that glacier at the beginning of the water year and h being glacier elevation at a given pixel, respectively. Note here that h, h_{max}, and h_{min} are *elevations*, not thicknesses like h_G.

In practice, applying the Δh parametrization requires (1) assigning an ID to each glacier for which the user would like to use the Δh parametrization (S3M expects this ID to be a positive integer); (2) mapping these glaciers ID on the simulation raster, so that S3M will be able to identify all pixels of the simulation domain belonging to a given glacier; (3) a-priori deriving Equation 42 for each glacier of interest and passing it to S3M as a pivot table, where Δh is sampled for a number of discretized h_r. S3M will then assign a Δh for each pixel of a given glacier using a nearest-neighbor interpolation of this pivot table. Both the glacier-ID map and the pivot table are part of the so-called static-data suite in input to S3M (Section **??** Supporting Information).

Once these preliminary steps are performed, S3M computes ice melt as in module G2, but h_G is not dynamically updated. Instead, ice melt for each pixel is accumulated to yield b_a, the cumulative mass balance in mm w.e. At the end of the water year, this information is used to compute factor f_s, which is employed to *scale* Equation 42 (the Δh profile) and so derive the actual change in glacier thickness for each glacier pixel:

$$f_s = \frac{\sum_{i=1}^{i=N_G} \left[b_{a,i} \times A_i \times A_{tot}^{-1} \right]}{\sum_{i=1}^{i=N_G} \left[\Delta h_i \times A_i \times A_{tot}^{-1} \right]} \tag{44}$$

where i denotes the i-th pixel of a given glacier, N_G is the total number of pixels of that glacier, A_i is the area of each pixel, and A_{tot} is the total area of the glacier. Once $h_{G,i} \to 0$, that pixel is excluded from all computations and h_{max} and h_{min} as well as all other variables are updated accordingly.

The general mass-conservation equation for glacier pixel i using G3 therefore reads:

$$IWE_{i,WY+1} = IWE_{i,WY} + SWE_{i,r} - f_s \Delta h_i, \tag{45}$$

with $SWE_{i,r}$ the residual snow water equivalent on that pixel at the end of the water year, while $IWE_{i,WY+1}$ and $IWE_{i,WY}$ are ice-water equivalent for piel pixel i during the current and the previous water year (WY), respectively.

The implementation of the Δh parametrization in S3M provides a number of modeling degrees of freedom. First, S3M assumes a non-dynamic mass balance for all pixels that are part of the model glacier mask, but have no glacier ID assigned; the user can explicitly choose this approach also for glaciers having a glacier ID, by setting all entries of the corresponding pivot table to -9999. This option is useful either where fitting a Δh parametrization is cumbersome (e.g., spatially incoherent glaciers) or for glacial remnants that are not moving anymore (e.g., glacierets). Second, the modeler can use different Δh parametrizations for various parts of the same large glacier, by simply assigning different glacier IDs to these parts and providing specific pivot-table entries for each ID. Also note that the Δh parametrization is bypassed whenever one glacier occupies only one pixel.

3 Case study: Aosta valley, NW Italian Alps

S3M is open software, including algorithms to prepare input data and set up computational environments and libraries. Links to all code are reported in the User Manual (see Section ?? the Supporting Information), with a general reference being CIMA Foundation's Hydrology and Hydraulics repository at https://github.com/c-hydro (Github organization).

This Section presents an application of S3M for an inner-Alpine valley located in north-western Italy (Aosta valley, Figure 3). This area has steep elevation gradients, with the main valley at elevations on the order of 300-400 m ASL and peaks as high as 4800 m ASL (Mont Blanc) or 4478 m ASL (Matterhorn). About 4% of Aosta valley is covered by glaciers (134 km^2), some of which are characterized by thick debris and develop for extend over several kilometers (e.g., the Miage glacier in the Mont-Blanc massif). With its cryosphere-dominated water supply and complex precipitation-topograghy interactions leading to marked rain shadows (Avanzi et al., 2021), Aosta valley is a formidable test bed for S3M.

S3M has been operational in Aosta valley since the early 2000s, as a component of a flood-forecasting chain called Flood-PROOFS (see Laiolo et al., 2014; Avanzi et al., 2021, and Section 2). This chain includes algorithms to spatialize and downscale weather-input data , of precipitation, air temperature, relative humidity, and radiation, automatically generate daily

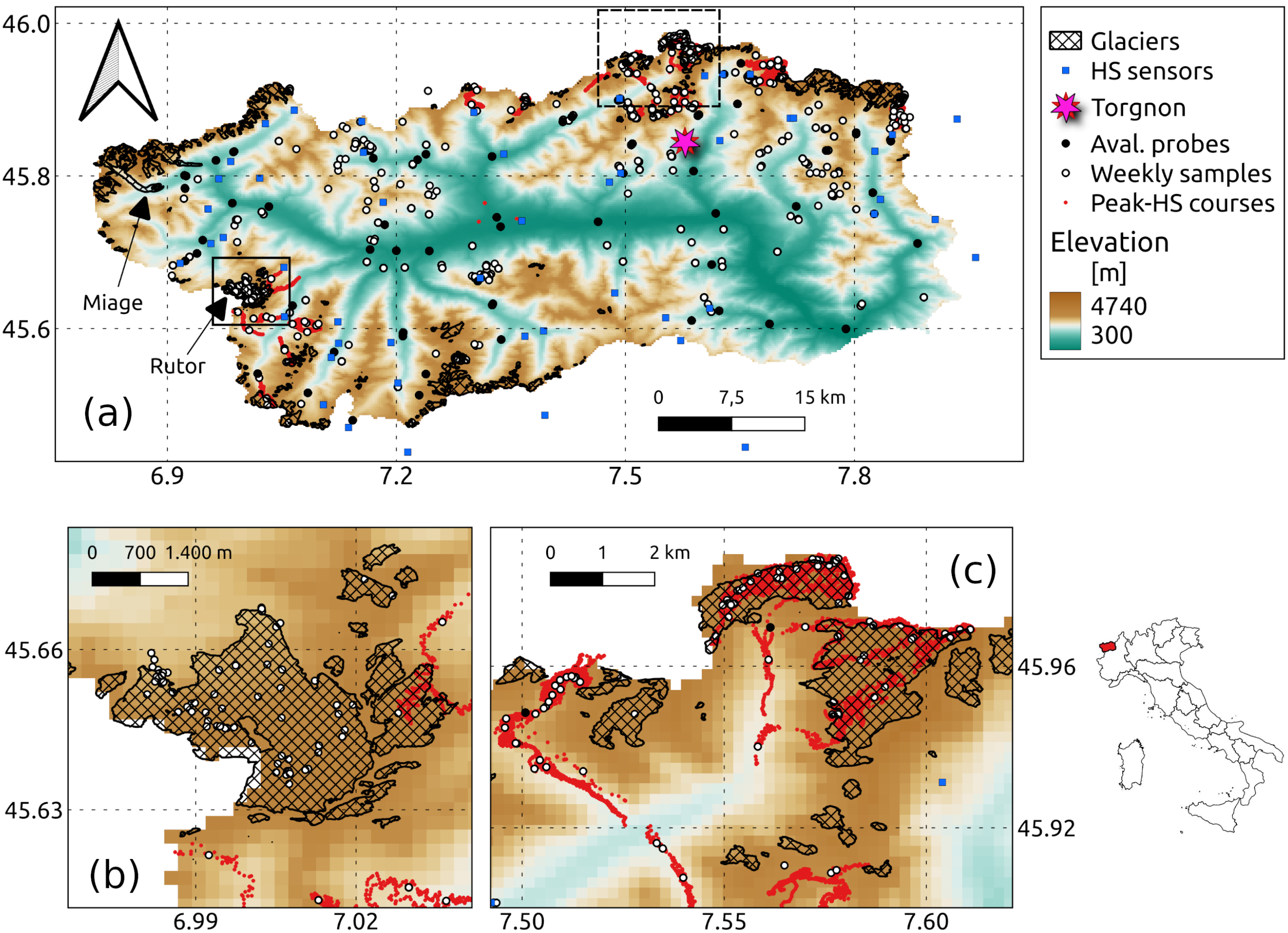

Figure 3. Aosta valley in north-western Italy. Panel (a): topography and glaciology of this region, with location of all snow-evaluation data used in this paper; panels (b) and (c): zoom on two intensive measurement regions, the Rutor glacier and the headwaters of Valpelline catchment, respectively. "HS sensors" are continuous-time snow-depth ultrasonic sensors, "Torgnon" is an intensive study plot with a variety of snow and weather datasets (see Section 3.3 and Terzago et al., 2019), ”Aval. probes” denotes locations of snow-depth measurements for avalanche-forecasting purposes, ”Weekly samples” denotes locations of ∼weekly snow-depth measurements collected mainly for water-supply forecasting, while “Peak-HS courses” are snow-depth measurements collected along transects of several kilometers for hydropower-forecasting purposes (see Avanzi et al., 2021, for more details). Panel (a) includes location of the Miage and Rutor glaciers, for which detailed evaluation results are reported in Section 3.5.

maps of snow depth and use MODIS snow-covered area, and process independently derived weekly maps of SWE (see the Supporting Information) . Together with runs of S3M in assimilation mode at ∼240 m spatial resolution, these tools inform real-time forecasts of streamflow at relevant closure sections obtained using the Continuum model (Silvestro et al., 2013)

(Laiolo et al., 2014; Avanzi et al., 2021) . Details about spatialization techniques and hydrologic modeling in Flood-PROOFS are available elsewhere (Boni et al., 2010; Laiolo et al., 2014; Avanzi et al., 2021) and are not discussed here for brevity. In the present paper, we instead leverage our application in Aosta valley to provide guidelines on how to calibrate S3M in a real-world case study (Section 3.1) and how to validate and interpret model results for the snow (Sections 3.2 to 3.4) and the glacier component (Section 3.5).

3.1 Calibrating S3M

In principle, a fairly large amount of S3M parameters can be calibrated, or at least fine-tuned based on expert knowledge. These parameters include the radiation and temperature snowmelt parameters m'_{rad} and m_r, the threshold temperature for inhibiting snowmelt (T_τ), the maximum weight of SWE-assimilation maps (W), as well as a number of climatological thresholds used to constrain model predictions (e.g., maximum and minimum snow density, or the snow-quality threshold to enable data assimilation, see Section **??** and Table **??** the Supporting Information). In practice, our experience suggests that the two melt parameters, m'_{rad} and m_r, are the prime calibration parameters of this model.

Because S3M is employed in assimilation mode in Aosta valley, and this mode includes MODIS snow-covered area, our calibration rationale focused on maximizing fit for point predictions rather than for spatial patterns. Still, calibration was performed considering open-loop simulations to avoid model performance to be spuriously driven by assimilation rather than parameter values. Calibration data comprised spatially distributed continuous-time measurements of 53 snow-depth sensors and temporally discontinuous manual measurements of snow depth collected across the region for water-supply or avalanche forecasting (see Avanzi et al., 2021, and Figure 3 for a data inventory). The calibration period covered water years 2010 through 2019, where the bulk of evaluation data was concentrated; the water year is a period between September 1 to August 31 and is indicated with the calendar year when it ends.

Our calibration protocol was based on performing multi-year simulations of S3M for a range of values of m'_{rad} and m_r: [0.8, 2] and [0.5, 1.5] mm °C^{-1} day^{-1}, respectively. These ranges were chosen based on preliminary tuning and, importantly, the notions fact that $m'_{rad} \sim 1.1$ implies a 100% efficiency of transmitted shortwave radiation in generating melt under likely isothermal conditions ($\bar{T}_{10d} \rightarrow 10$°C, see Figure 2(a) and Section 2), while $m_r \sim 1.4$ tallies with previous work by Pellicciotti et al. (2005). The parameter space was explored for increments of 0.025 of m'_{rad} and 0.05 mm °C^{-1} day^{-1} of m_r, and we first calibrated an optimal value of m'_{rad} and then of m_r. This meant running 29 decade-long simulations for all tentative values of m'_{rad}, finding the optimal one, and then re-running 25 simulations tuning m_r. This sequential calibration approach is only one out of several possible calibration approaches, including strategically exploring the parameter space (Razavi et al., 2019) . Here, we chose a sequential approach for this illustrative case study mainly for computational-resource constraints.

As objective metric, we minimized $Obj(\Theta) = 0.5 \times (1 - \mathrm{KGE}(\Theta)) + 0.5 \times (\mathrm{RMSE}(\Theta))/\overline{\mathrm{RMSE}(\Theta)}$, with Θ being the generic parameter value, KGE being the Kling-Gupta Efficiency metric as defined in Kling et al. (2012), RMSE being the Root Mean Square Error, and $\overline{\mathrm{RMSE}(\Theta)}$ being the mean RMSE across all parameter values. This objective metric was chosen to combine the features of KGE (and in particular its focus on correlation, bias, and ratio of coefficients of variation) with a specific weight for large errors (RMSE). The RMSE was normalized by its mean across all parameter values to make it adimensional and so comparable to KGE. For each parameter value Θ, Obj was computed between observed snow depth (Figure 3) and simulated h_S, both merging all data from all years in one sample and separately for each water year (all-years and yearly values, respectively).

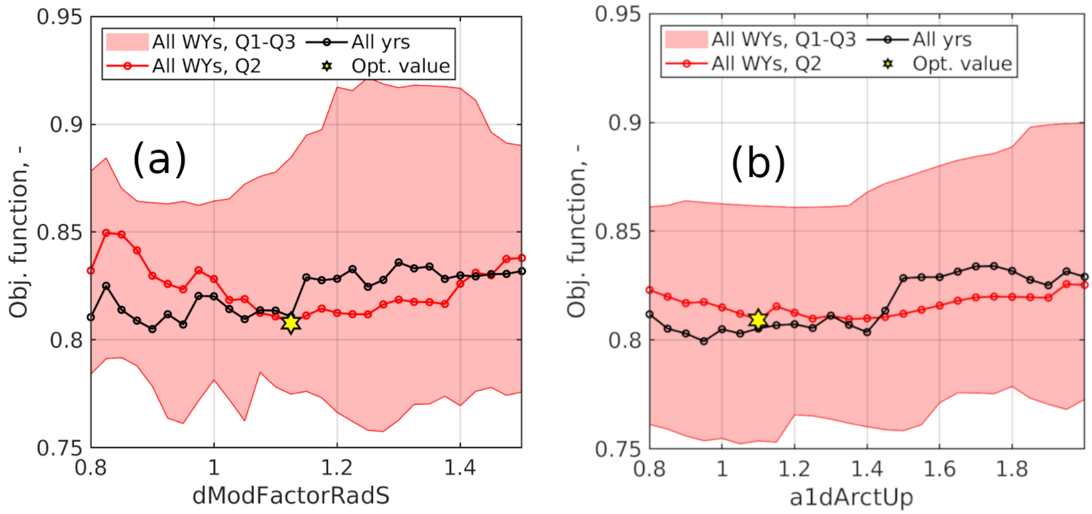

Figure 4. Calibration objective metrics as a function of parameter values, with dModFactorRadS being m'_{rad} and a1dArctUp being m_r (see the Appendix Supporting Information for details on model's notation in the source code). Parameter m'_{rad} is adimensional and m_r is in mm °C^{-1} day^{-1}. For each parameter value Θ, the objective metric was computed using both all data from all years in one sample and separately for each water year (all-years and yearly values, respectively). Q1, Q2, and Q3 are the first, second, and third quartiles of objective metrics across all water years. WY is water year.

Median yearly values across all water years show a minimum for $m'_{rad} = 1.125$ and then $m_r = 1.10$ mm °C^{-1} day^{-1}, in line with expectations (Figure 4 and Section 2). Objective-metric values showed remarkable variability across water years (see the quartile range in Figure 4), owing to significant variability in the original sample of snow-depth values between warm and cold years (Avanzi et al., 2021). Thus, multi-year calibration periods are recommended, although the range of variability in median and all-year Obj in Figure 4 suggests that the sensitivity of S3M to m'_{rad} and m_r is surprisingly low, especially if one considers that calibration-based snow models are prone to large drops in performance outside the calibration sample (Hock, 2003; Avanzi et al., 2016). We interpret this to be because of the hybrid physics-based and temperature-index approach employed in S3M to predict snowmelt (Equation 15), which appears to better constrain parameter values than a purely temperature-index approach because it brings S3M closer to a first-principals energy balance model .

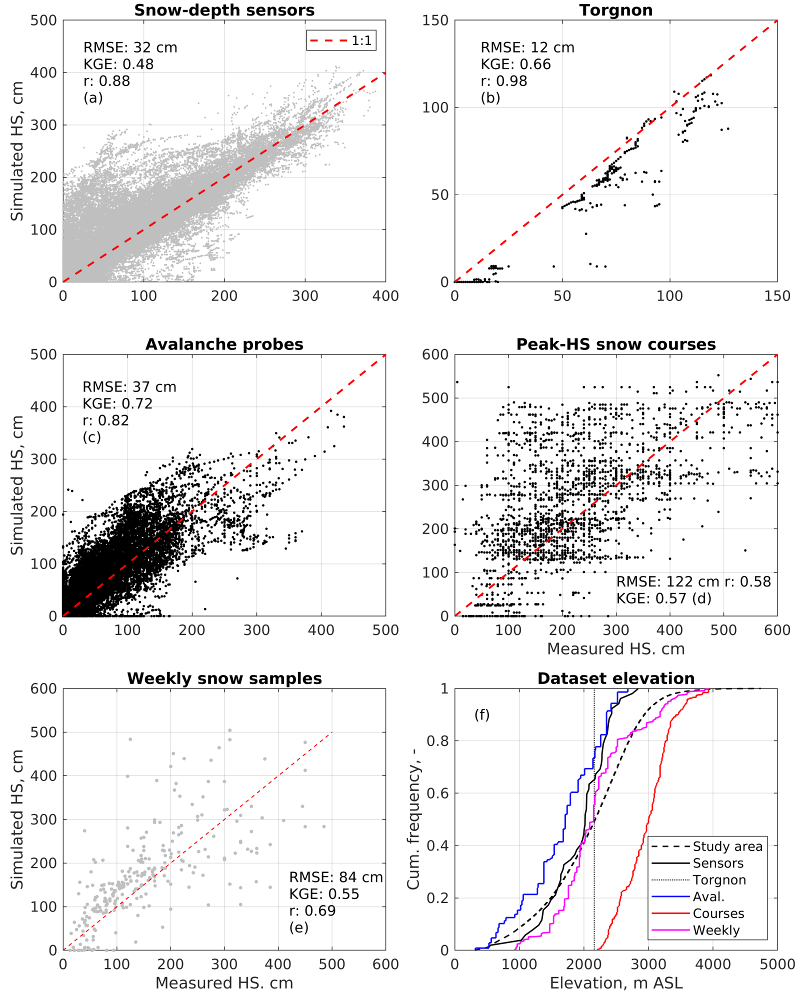

Figure 5. Performance of S3M in simulating point snow depth, as measured by continuous-time snow-depth sensors (a), the snow-depth sensor at the intensive study plot of Torgnon, and manual snow-depth measurements taken for avalanche, hydropower, and water-supply forecasting (c to e). Because simulations were carried out in assimilation mode, and assimilated maps indirectly involved snow-depth sensors and weekly snow samples, performances for these datasets are reported only for reference. Panel (f) shows the elevation distribution of each dataset and of Aosta valley for context. RMSE is Root Mean Square Error, KGE is the Kling-Gupta Efficiency (Kling et al., 2012), and r is Pearson's correlation coefficient. The spatial resolution of snow courses (panel d) is much finer than that of the model (say, ∼60 m vs. ∼220 m, respectively), thus a number of snow-course data were compared to the same modeling value. This explains the occurrence of sharp, horizontal lines in panel (d).

3.2 Evaluation: point snow depth

Figure 5 show simulated vs. observed snow depth (symbol HS per guidelines by Fierz et al., 2009) for the 52 snow-depth sensors in Figure 3, the snow-depth sensor at the Torgnon study plot, as well as for all manual snow-depth measurements taken for avalanche, hydropower, and water-supply forecasting (panels a to e, respectively). The evaluation period in Figure 5 and all the remaining sections of this paper is water years from 2004 to 2009 and 2020, that is, all years before and after the calibration period in Section 3.1. Simulations in this and following Sections sections were carried out in assimilation mode, as this is the approach we generally use in real-time forecasting and so results are more representative of real-world model performance. More details on this assimilation procedure are reported in Avanzi et al. (2021); note that snow-depth assimilation maps are only generated between August and April in an effort to unaffect the simulation of the depletion phase of the seasonal snowpack.

Snow-depth-sensor and weekly-snow-sample measurements in Figure 5(a) and (e) were indirectly assimilated in S3M as they are involved in the computation of the so-called Updating and weekly-SWE maps (see Section 2), meaning their performance statistics are only reported for reference. Non-assimilated data at Torgnon (Figure 5(b)) and from avalanche probes (Figure 5(c)) maintain comparatively high values of RMSE and KGE (12-37 cm and 0.66-0.72, respectively), with no evident tendency for systematic under- or overestimations. Open-loop results were not reported here for brevity, but generally show comparable performance for these datasets. Thus, we conclude that our calibration strategy not only showed little sensitivity of the model to m'_{rad} and m_r (Figure 4), but also led to a robust performance across nearly twenty water years and for areas that were not included in the calibration pool.

Peak-snow-depth courses show a significantly lower performance, in particular in terms of a larger dispersion around the 1:1 line, a larger RMSE (122 cm), and a lower KGE (0.57, (Figure 5(d)). This is because this course dataset comprises snow-depth measurements at significantly higher elevations than any other considered dataset (see elevation distribution in Figure 5(f)). At those elevations, both interactions between the snowpack and topography complicates snow distribution compared to low-elevation areas, and density of input-data stations is much lower (Avanzi et al., 2021). Still, the fact that S3M does not show any obvious over- or underestimation for those elevations is encouraging for our scopes, also considering the comparatively coarse resolution of our implementation in Aosta valley (∼240 m).

3.3 Evaluation: the Torgnon study plot

S3M satisfactorily reproduces the timing of peak accumulation and so the onset of the snowmelt season at the Torgnon study plot, both in terms of snow depth (h_S) and SWE (Figure 6). , this Figure includes a mixture of calibration - 2013-2019 - and evaluation - 2020 - water years). In this regard, Kling-Gupta Efficiency for snow depth and SWE is ∼ 0.70 and ∼0.84, respectively. Discrepancies between observed and simulated snow depth increase in spring, mainly because spatial heterogeneity in snow depth increases during the snowmelt season (Grünewald et al., 2010) and this challenges the comparison between a point measurement of snow depth and our 240-m snow model (this could be improved by increasing model resolution). Overall,

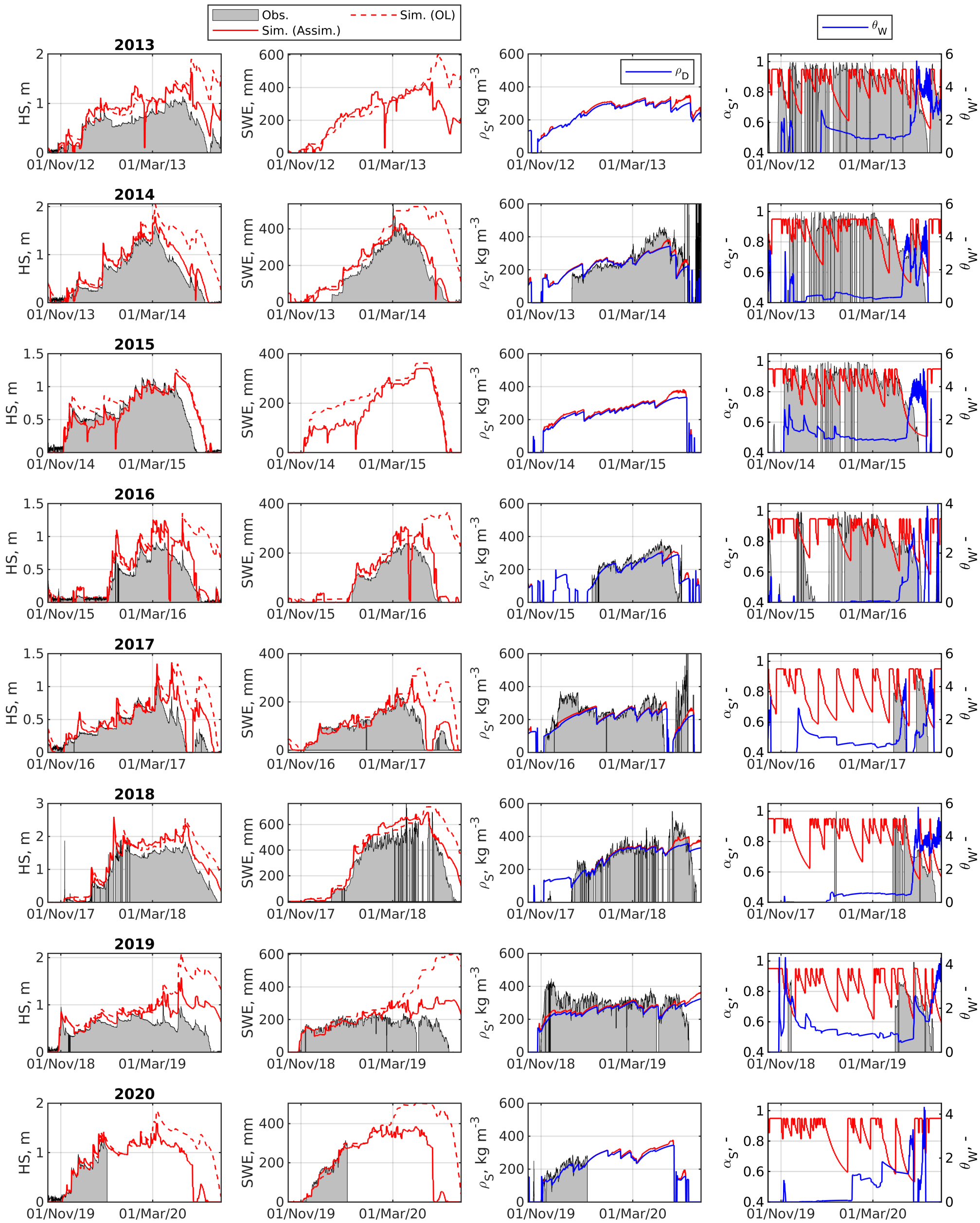

Figure 6. Comparison between measurements and modeling outputs at the Torgnon study plot. First, second, third, and fourth columns are snow depth (HS), SWE, bulk-snow density, and albedo, respectively. The third and fourth columns also report dry-snow density and bulk volumetric liquid-water content, respectively. Each row is one water year (2013 to 2020).

the model correctly captures snowmelt rate and peak SWE for most water years, which are the primary variable of interest in operational snow hydrology.

Sporadic, yet abrupt oscillations in snow depth or SWE in the assimilated simulation are due to the assimilation dataset, which is the operational result of a multiregression model fitted across observed snow depth at ultrasonic-sensor stations and a number of physiographic features (Avanzi et al., 2021). These regressions often maintain – or even propagate – measurement noise, a frequent issue of ultrasonic snow-depth sensors (Ryan et al., 2008). On the other hand, open loop simulations do not display the same abrupt oscillations, which validates model's parameterizations.

S3M also reproduces the magnitude of bulk-snow density and its increase with time for all water years (Figure 6), in agreement with previous models implementing a similar parametrization of snow settling (De Michele et al., 2013; Avanzi et al., 2016) and despite its one-layer approach. Values of bulk and dry snow density are very close to each other during the accumulation season, while the latter diverges from the former during the snowmelt season. This is due to an increase in mass for the wet component of the snowpack during spring, as confirmed in terms of bulk liquid-water content (Figure 6). The seasonal range of variability for modeled bulk liquid-water content and its peak around 5 vol% during the snowmelt season agree with measurements by Techel and Pielmeier (2011); Heilig et al. (2015); Avanzi et al. (2017) and the international classification by Fierz et al. (2009).

The Torgnon study plot also measures incoming and reflected short-wave radiation, which allowed a comparison in terms of measured and simulated albedo (Figure 6). During the accumulation season, measured albedo is generally higher than simulated albedo; in particular, both measured and simulated albedo show maximum values around 0.95, but only the latter decreases well below 0.8-0.7 between snowfall events. Simulations by SNOWPACK at the same study plot (Terzago et al., 2019, not reported for brevity) qualitatively showed higher values than S3M, evidence that only relying on time as a predictor of albedo may yield frequent underestimations compared to a model that considers a broader spectrum of albedo predictors like SNOWPACK. On the other hand, S3M well captures the measured decline in albedo during the snowmelt season, which, again, is important to capture the timing and intensity of seasonal melt.

3.4 Evaluation: snow distribution

Figure 7 shows a simulated reanalysis of the 2019-20 snow season, which well exemplifies the information and level of details provided by S3M to forecasters (note that this snow season is part of the validation pool) . The 2020 snow season started by the end of October 2019 (Figure 7(a)), with largely uninterrupted precipitation events between November and December 2019 leading to nearly 75% of spatially average SWE across Aosta valley being accumulated before January 2020 (Figure 7(b)). January and February were relatively dry months, with only one warm storm in mid-February and then a cold one between February and early March 2020. The snowmelt season started in April, even though $\sim$40% of spatially averaged SWE at high elevations persisted by the end of May 2020. The season was characterized by an alternation between cold and warm spells, which led to frequent melt-freeze cycles in the spatially averaged snowpack (Figure 7(b)).

The spatial distribution of SWE confirmed an increase in snow accumulation between 15 December (Figure 7(c)) and 6 March (Figure 7(d)), with the expected positive gradient with elevation. Simulations for 20 April 2020 showed a typical

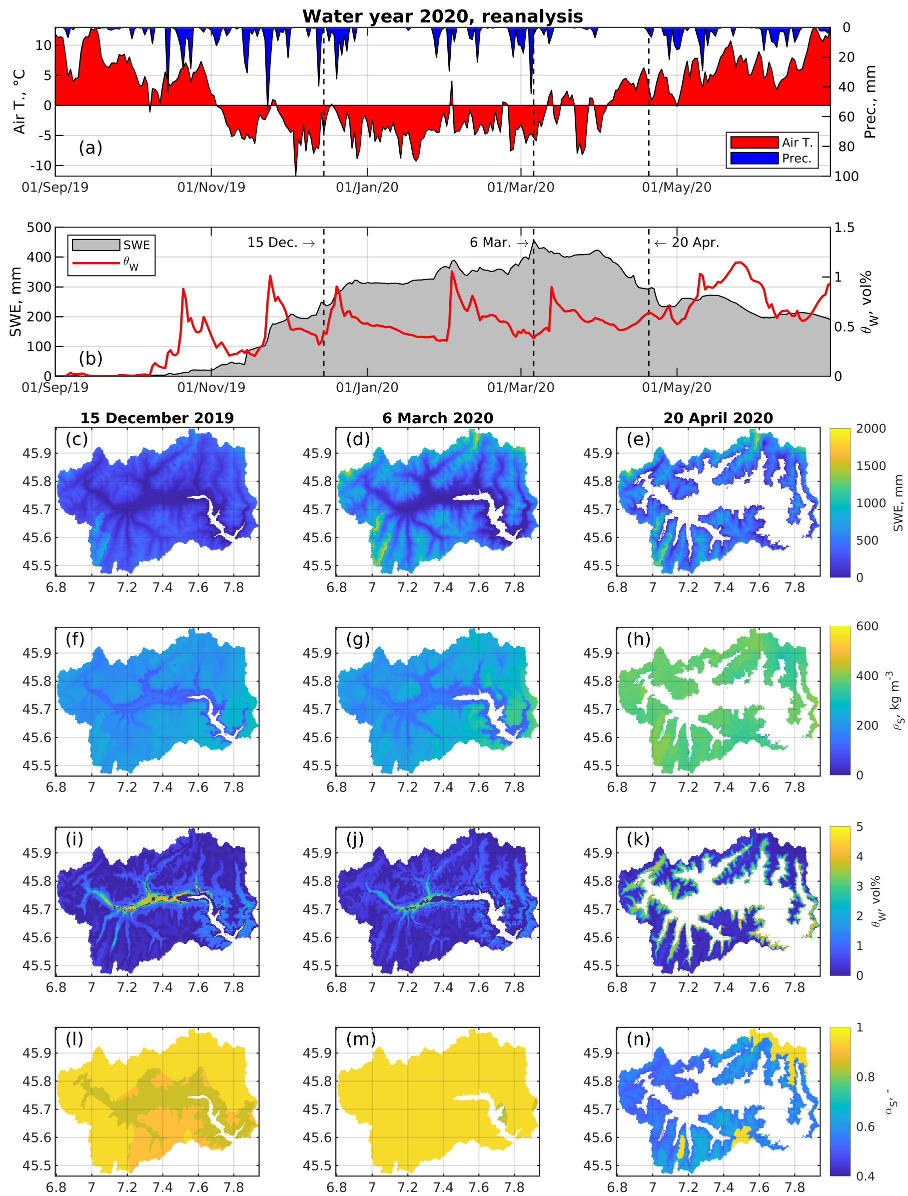

Figure 7. Simulated reanalysis of the 2020 snow season: spatially average air temperature and total precipitation (a), spatially average SWE and bulk liquid-water content θ_W (b), and distribution of SWE (c-e), bulk snow density ρ_S (f-h), bulk liquid water content (i-k), and albedo α_S (l-n) for three example dates: 15 December 2019 (first column), 6 March 2020 (middle column), and 20 April 2020 (third column). Statistics in panel (a) and (b) are spatially averages across the entire Aosta Valley region.

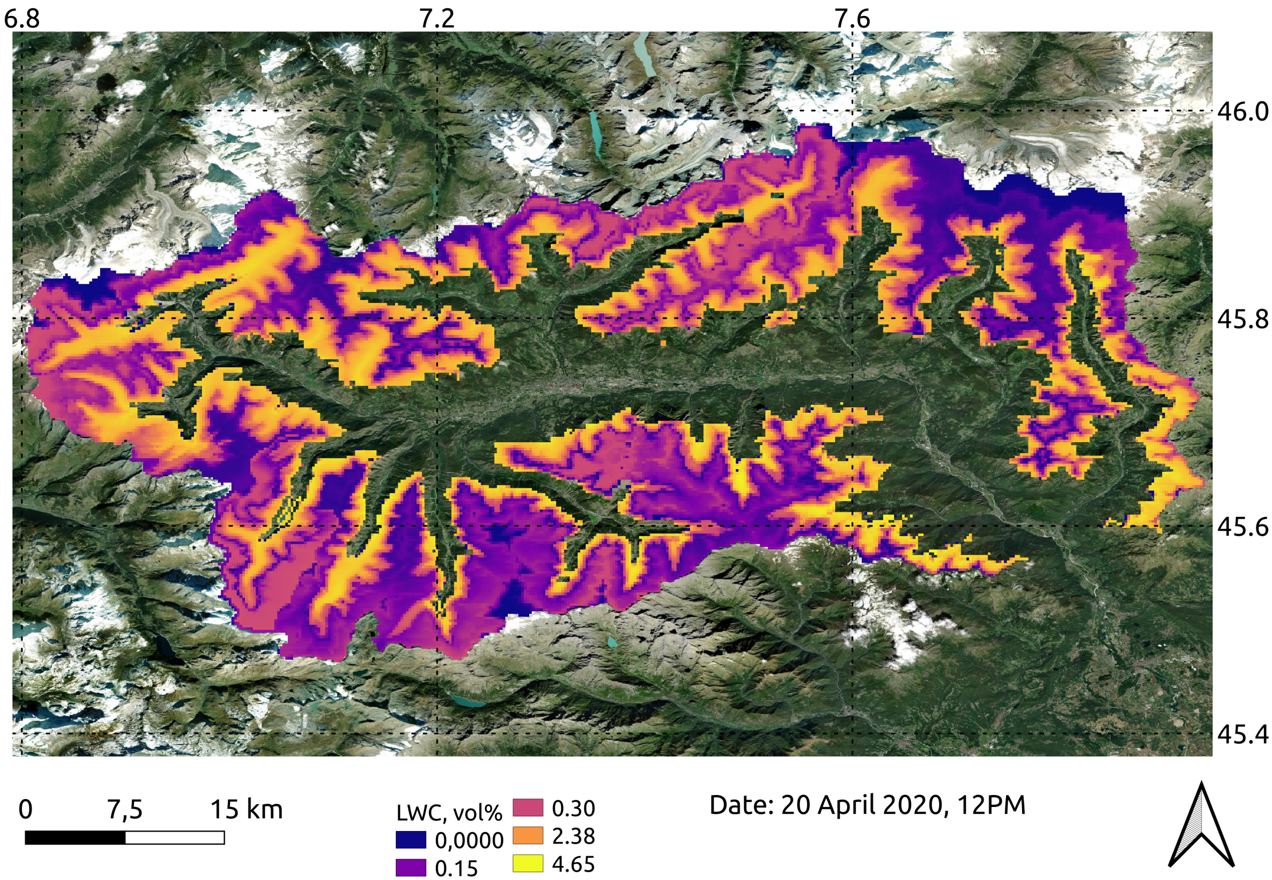

Figure 8. Map of bulk volumetric liquid-water content for Aosta valley (LWC, same as θ_W), 20 April 2020 at 12PM. Background layer is from the ESRI Satellite theme.

snapshot of the snowmelt season, with largely depleted snowpack at low and medium elevations and SWE still on the order of 1000 - 1500 mm at elevations above 3000 m ASL. Depletion was spatially more extensive on south-facing slopes compared to north-facing slopes, due to topography-radiation interactions.

Bulk-snow density was spatially fairly homogeneous, especially at the beginning of the snow season (Figure 7(f)). With time, some differences emerged, with snow density increasing faster in areas with both larger SWE and likely warmer temperatures (Figure 7(g) and (h)). Both the magnitude of snow-density values in Figure 7 and the fact that this variable was spatially more homogeneous than SWE tallies with previous works (López Moreno et al., 2013).

Maps of bulk-liquid water content were largely influenced by local climate, with a general rise in wetness with decreasing elevation that closely followed local topographic contours and aspect (Figure 7(i) to (k) and see Figure 8). Overall, bulk liquid-water content around the snow line was larger in April than in December or March, which again tallies with expected seasonal trends in wetness (Techel and Pielmeier, 2011). While liquid water in snow has been investigated for a long time

(Colbeck, 1971), recent work on wet snow provides renovated new opportunities for considering bulk liquid-water content from an operational standpoint, whether to predict the onset of snowpack runoff (Wever et al., 2014) or wet-snow avalanches (Wever et al., 2016). Recent (Mitterer et al., 2013; Wever et al., 2016). Early evidence that wet-snow conditions have increased in frequency and have extended well into the winter season due to a warming trend (Pielmeier et al., 2013) further justifies interest in spatially explicit, raster-like predictions of wet-snow patterns wet snow predictions like those in Figure 8. While application to significantly changed conditions will necessarily require some forms of parameter tuning or recalibration, S3M is among the first few parsimonious snow models to provide such information spatially explicit, raster-like predictions of wet-snow patterns .

Maps of albedo showed the expected homogeneity during the accumulation season, owing to frequent snowfall events between November and March (Figure 7(l) and (m)). On the other hand, albedo in spring was much lower and spatially more diverse than in winter, with residual high values across the highest peaks of Aosta valley and values well below 0.6-0.7 in areas covered by older and wetter snow.

3.5 Evaluation: glacier evolution

The dataset considered while evaluating S3M in Aosta valley comprised 94 ablation-stake measurements collected between 2009 and 2015 across the Rutor, Timorion, and Petit Grapillon glaciers (Figure 9). These are all high-elevation, debris free glaciers of various size (7.91 km^2, 0.48 km^2, and 0.18 km^2, respectively – 2012 data), thus providing a representative sample to test the accuracy of S3M in capturing glacier ablation (note that these measurements were not included in the calibration of S3M, so they are a validation dataset) . Simulations using the G3 glacier module (that is, including the Δh parametrization) returned solid satisfactory results in this regard, with a correlation between simulated and observed change in thickness of 0.6 (Figure 9(d)). The correspondence between simulated and observed change in thickness across the total range of variability in measurements was visually higher for the Rutor glaciers than for the Timorion and the Petit Grapillon, which we interpret because of the large size of the first compared to model resolution (240 m). Also, the number of available samples for the Rutor is significantly larger than for the Timorion and the Petit Grapillon, meaning the ; for the latter, glacier surveys are challenged by extensive and deep crevasses, as well as frequent avalanches, that make point measurements non-representative of the actual melt pattern. Thus, the performance observed for the former Rutor glacier is likely more representative of S3M predictive skills.

The evolution of glacier thickness for the Rutor glacier shows expected spatial patterns, with minor ablation at elevations above 3000 m ASL and progressively more intense melt close to the terminus below 2750 m ASL (Figure 10, see Figure 3 for location of this glacier in the study region). Annual changes show significant interannual variability, with somewhat more intense melt as the evaluation period progresses; in any case, the spatial pattern is preserved as hypothesized by the Δh parametrization. At elevations above 3200 m ASL, glacier thickness increased owing to snow-to-ice conversion.

Figure 11 shows similar spatial patterns for one of the most complex glaciers in the Alps, the Miage glacier, a 10.8-km^2 (2012), 10-km+ long valley glacier covering a $\sim$ 2000-m elevation range of the Mont Blanc massif (see Figure 3 for location of this glacier in the study region) . Like many other valley glaciers across the southern Alps (Diolaiuti et al., 2003), vast portions

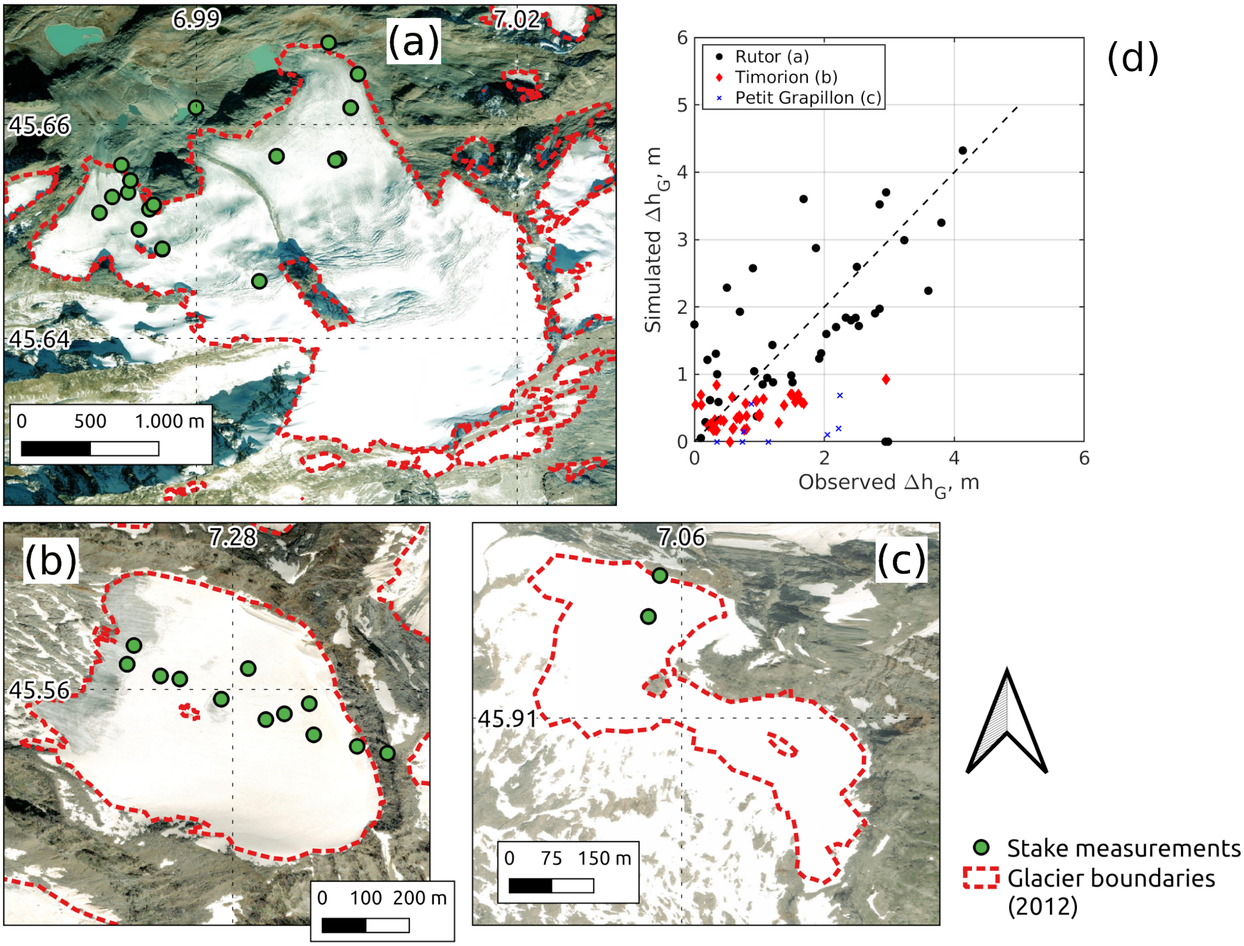

Figure 9. Spatial distribution of glacier-ablation measurements across the Rutor (a), the Timorion (b), and the Petit Grapillon (c) glaciers in Aosta valley. Panel (d) shows a comparison between measured and simulated ablation (positive values mean a decrease in local ice thickness). The number of points in panel (d) does not correspond to the number of stake locations in panels (a) to (c) because of repeated measurements taken cross multiple water years as the same stake location. Background layer is from the ESRI Satellite theme.

of the Miage tongue are covered by debris, which has been shown to lead to below-debris melt being insensitive to variations in atmospheric temperature (Brock et al., 2010). Albeit hard to validate due to a lack of measurements, our implementation of the Miage glacier qualitatively captured this disconnection between intense melt across medium-elevation areas with little to none known debris and low melt rates in areas close to the glacier terminus that are well known to be covered by thick debris (Figure 11). Thanks to supporting a spatially explicit debris-driven melt factor (Equation 40), S3M yielded estimates of thickness change that were much more spatially diverse and less correlated with elevation on the Miage than on the Rutor glacier (and so much less correlated with elevation, correlation coeffients of 0.95 and 0.85, respectively, compare Figure 11

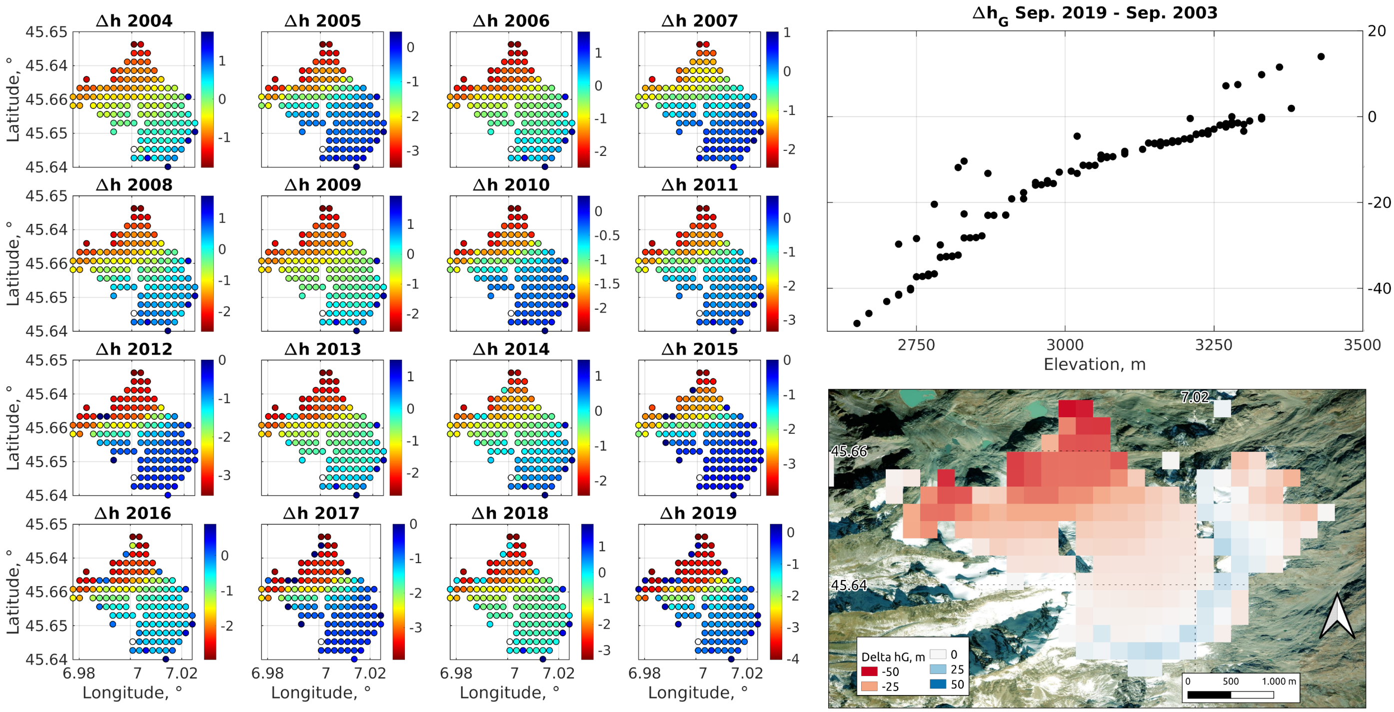

Figure 10. Rutor glacier: spatial patterns of annual change in glacier thickness (left), cumulative change in glacier thickness between September 2003 and 2019 as a function of pixel elevation (right, top), and spatial distribution of this cumulative change (right, bottom). Background layer is from the ESRI Satellite theme.

with Figure 10). At elevations above ∼3000 m ASL, debris is residual if non-existent, and so change in thickness and elevation maintained the same high correlation observed on the Rutor glacier in Figure 10.

4 Applicability and future developments

As a hydrology-oriented cryospheric model, S3M delivers timely and computationally efficient predictionsof the most significant features of the cryosphere water budget, while still aiming at a comparatively high standard in physical realism , while aiming at including the most salient processes of snow and glacier hydrology . Understanding this trade-off and its implications is important to determine model applicability and adequacy in a given context.

The structure and state variables of the model are all geared toward providing decision-relevant information for water-supply forecasting, which remains the prime area of application tested by the authors (Laiolo et al., 2014). In this context, typical questions that S3M contributes to answer are: how much snow-water resources are currently accumulated across the landscape? What headwater regions are currently releasing meltwater, and what are still accumulating snowpack? When a certain percentage of the seasonal freshet is expected to reach a given closure section? Are glaciers currently contributing

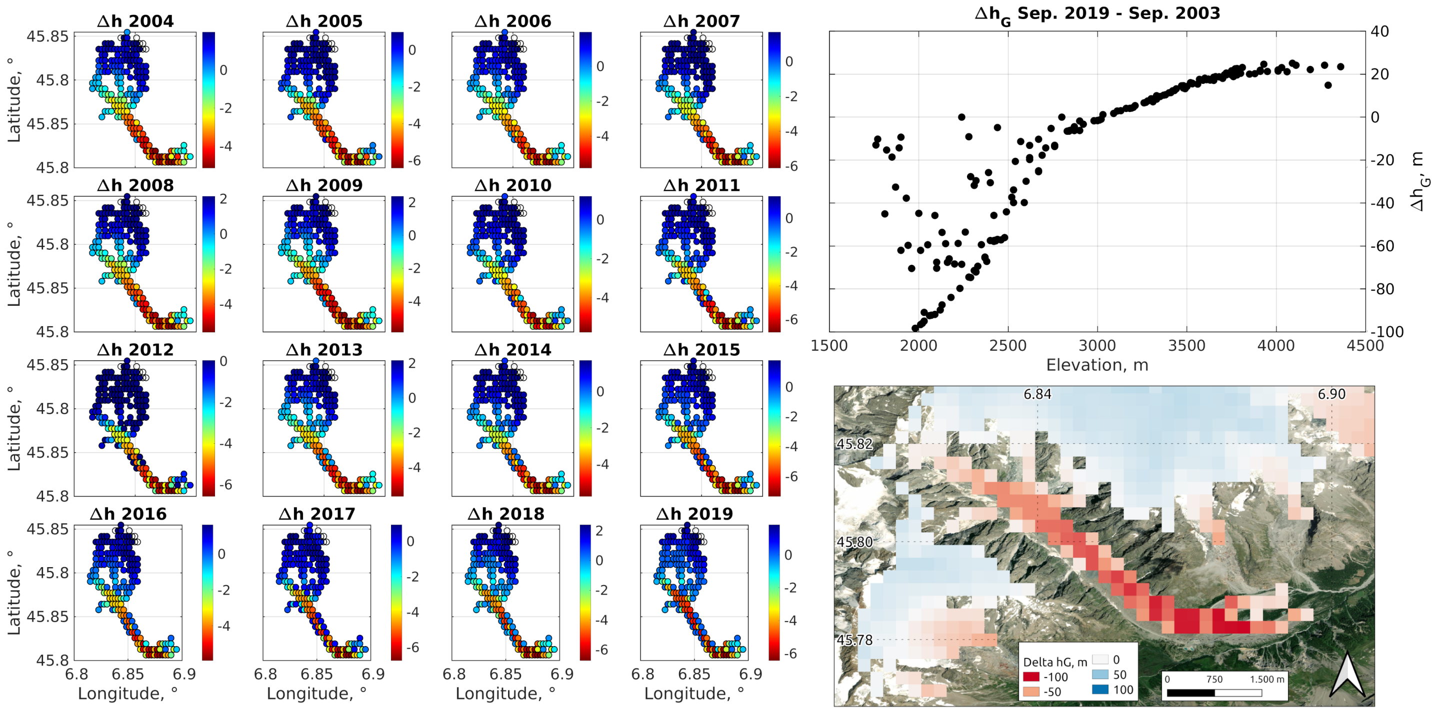

Figure 11. Miage glacier: spatial patterns of annual change in glacier thickness (left), cumulative change in glacier thickness between September 2003 and 2019 as a function of pixel elevation (right, top), and spatial distribution of this cumulative change (right, bottom). Background layer is from the ESRI Satellite theme.

runoff, and if so how much is their relative contribution? Decisions that are currently being informed by S3M thus range from flood-forecasting early warning to hydropower planning. S3M also provides some support to avalanche hazard forecasting, but this remains an unexplored area of application for which the microstructural detail in this model is largely insufficient.

Recently, we also started using S3M to produce future scenarios of water resources in mountain regions. Two attractive features of S3M in this regard are the comparatively limited computational times of this model and the inclusion of both snow and glacier mass balances. Regarding the former, computational time for one water year worth of simulations in Aosta valley runs in the hours for an ordinary laptop with a few hours for a laptop with six i7 8th-generation cores and solid-state storage (240 m resolution, $\sim$3290 km^2). Storage type is a factor here because S3M includes access to, and creation of, input and output NetCDF files (see the Appendix Supporting Information), and the frequency and size of output files in particular play a key role in determining computational time. Regarding snow and glacier mass balances, models providing even medium-level physical realism of both these features are still rare , not to mention the scarcity of open-source suites reconnecting them with the hydrologic cycle and so with streamflow predictions (Bongio et al., 2016; Li et al., 2015). (Bongio et al., 2016; Li et al., 2015). Thanks to its integration with the Continuum hydrologic model (also open source, see Silvestro et al., 2013), S3M can deliver such mass-conserving and spatially consistent predictions of the entire mountain water budget.

S3M is currently being actively maintained and further developed, with four five main areas of planned future work. The first is the inclusion of wind effects, both as an additional component of the energy balance and as a driver of snow redistribution (wind drift). Explicitly including wind in the energy budget is particularly urgent given that turbulent fluxes are a key contributor to melt during flood-generating rain-on-snow events (Marks et al., 1998; Würzer et al., 2016). As for wind drift, advances in this context are warranted not only in terms of relocation of blowing snow in the form of suspension, saltation, and creep (DeWalle and Rango, 2011), but also (and likely more importantly) in terms of the associated sublimation. Progress in this regard has been hampered by a lack of detailed measurements of wind across the complex terrain of mountain headwaters, but the publication of recent datasets in this regard may favor future work on this topic (Guyomarc'h et al., 2019).

A second area of planned future work regards the inclusion of vegetation effects on the snowpack. The science of canopy-snow interactions has identified four mechanisms through which vegetation can alter snowpack evolution compared to open areas: precipitation interception and throughfall, shortwave radiation shadowing, longwave-radiation enhancement, and wind shielding (Rutter et al., 2009). While the importance of each of these mechanisms for the fate of a seasonal snowpack dramatically changes with local climate (Lundquist et al., 2013), scientific consensus is that canopy may reduce peak SWE by more than 50% and lead to perturbations in the melt-out date on the order of weeks (Rutter et al., 2009), depending on canopy or snow-fractional cover. Helbig et al. (2020) have recently proposed a parsimonious parametrization for canopy effects in large scale models, thus providing a solid starting point to include these processes in S3M.

The third direction of future development is liquid-water transport in snow, a rarely parametrized but important connection between surface melt and snowpack runoff. Water infiltration through snow manifests itself as both spatially homogeneous matrix flow and spatially heterogeneous preferential flow (Katsushima et al., 2013), with transition between these two regimes being driven by wet-snow metamorphism and snow properties like density and grain size (Avanzi et al., 2017; Hirashima et al., 2019). While capturing such micro-scale mechanisms is likely beyond the scope of a large-scale, distributed model, including some forms of preferential flow in S3M will likely enhance its performance in terms of timing and peak of early-season snowmelt events or rain on snow (Wever et al., 2014; Würzer et al., 2017). A way forward in this regard may be the simple parametrization originally proposed by Katsushima et al. (2009), which models preferential-flow discharge as a θ_W-driven threshold process. Another important aspect here is slope flow, that is, the tendency of snow to redistribute meltwater along layer boundaries for distances of hundreds of meters downhill (Eiriksson et al., 2013; Webb et al., 2018). Both measurements and consequently parametrizations of this process are still very rare, and more work is needed before this process can be included in parsimonious models like S3M.

Fourth, the conversion from snow to ice in S3M is very simplified, and completely skips the intermediate stage of firn (Cuffey and Paterson, 2010). While we usually turn off the glacier-mass balance when using S3M in flood forecasting, and while accumulation of multi-year snow as firn will likely characterize only very high elevations in a warming climate, this transition is still an important process to capture from the perspective of physical realism. Considering firn may also extend the applicability of S3M to polar regions, where for example firn-storage capacity is an important factor in determining the long-term fate of the Greenland ice sheet (Forster et al., 2014; Machguth et al., 2016). In this regard, Banfi and De Michele (2021) have recently proposed a local model of snow-firn transition for a binary-mixture snowpack like that considered in S3M.

Fifth, more work is planned to improve the data-assimilation component of S3M, particularly in terms of widening the array of state variables for which assimilation is supported (currently, SWE and snow depth) and in terms of improving assimilation data themselves. Regarding the former, the field of multivariate data assimilation is ripe (Piazzi et al., 2018), although scaling up these approaches across the landscape may come with significant computational requirements. Regarding new assimilation data, statistical learning is making promising steps towards mining new information from traditional, sometimes even sparse and fuzzy data across geosciences (Avanzi et al., 2019; Ghanjkhanlo et al., 2020; Revuelto et al., 2020; Dramsch, 2020; Grossi et al., 2021 . Meanwhile, Cluzet et al. (2020) has showed some degree of success in assimilating satellite reflectance into snowpack simulations as a way to better capture snow microstructure and so the energy balance. Lessons learned from these recent advances will be incorporated in future releases of S3M.

5 Conclusions

We presented S3M v5.1, a spatially explicit hydrology-oriented cryospheric model that successfully reconstructs seasonal snow and glacier evolution through time. The model comprises parametrizations for precipitation-phase partitioning, snow and glacier energy and mass balances, snow rheology and so density evolution, snow aging and albedo, and various a hybrid temperature-index and radiation-driven melt parametrization, and provisions for data assimilation. Overall, the model channels elements from the state of the art in cryospheric sciences into a parsimonious and computationally efficient model. Regarding snow, specific elements of relative novelty in this regard are an explicit representation of snow liquid-water content and a hybrid physics-based and temperature-index approach to snowmelt that decouples the radiation- and temperature-driven contributions. The glacier component also includes the well-known Δh parametrization and the possibility to feed the model with a distributed debris-driven melt factor, both comparatively new approaches in the field. S3M provides an open-source platform to simulate snow and glacier dynamics with the necessary physical realism for hydrologic purposes. Together with the hydrologic model Continuum (Silvestro et al., 2013), S3M fulfills the recurring need for integrated glacio-hydrologic models in both scientific research and operational practice, and can provide the basis for more robust, large scale predictions of the fate of the cryosphere at multiple time scales — from hours to centuries ahead.

Code availability. The S3M snow model is available on CIMA Foundation's Hydrology and Hydraulics repository at https://github.com/c-hydro/s3m-dev (GitHub organization), including algorithms to prepare input data and set up computational environments and libraries. S3M is also available on Zenodo at https://doi.org/10.5281/zenodo.4663899.

Data availability. Data used in this paper are available through the Aosta Valley Regional Authority, the Snow and Avalanche Office (Ufficio Neve e Valanghe - RAVDA), and the Aosta Valley Environmental Protection Agency.

Author contributions. FA, SG, FD, and FS developed S3M v5.1, with contributions from various colleagues over the course of the last ∼15 years. FA carried out model evaluation in Aosta valley, with inputs from SG, EC, UMdC, SR, and HS. EC and UMdC collected snow-course and glacier data and shared general knowledge about cryospheric processes in the study catchments. SR and HS provided weather and snow data collected by the Aosta Valley Regional Authority, as well as shared general knowledge about hydrologic processes in the study catchments. FA prepared the manuscript, with inputs from all coauthors.

Competing interests. Authors declare no competing interest.

Acknowledgements. This work was supported by the Aosta Valley Regional Administration, the Italian Civil-Protection Department, and CVA S.p.A. The authors also would like to thank all colleagues who contributed to developing previous versions of S3M over the course of the last ∼15 years. Fruitful discussions during the development of S3M v5.1 with Matthias Huss, Bettina Schaefli, and Biagio Di Mauro are acknowledged. Authors also thanks the Aosta Valley Regional Authority, the Snow and Avalanche Office (Ufficio Neve e Valanghe - RAVDA), and the Aosta Valley Environmental Protection Agency for validation data.

6 User Manual

5.1 Run preparation

S3M v5.1 requires two categories of input, compulsory data: **dynamic**, weather and **static**, topographic inputs. Optionally, the model also ingests **assimilation** data, in the form of either snow-depth and SCA maps or SWE maps (Updating and SWE maps, respectively, see Section 2). The format file required by S3M v5.1 for all inputs is the NetCDF format in the standard GNU zip compression algorithm (gzip, extension .nc.gz).

5.0.1 Static data

Mandatory static data include:

- a Digital Elevation Model (DEM, in m ASL);
- a raster with metric areas of each computational-grid cell (so-called AreaCell, in m^2);
- a glacier mask.

These static rasters must have the same geographic grid and reference system, which will define the computational grid of the model. The glacier mask will indicate which pixels are covered by glaciers, using a unique integer identifier that is passed through the parameter list (so-called Namelist or Infofile, see below for details). S3M v5.1 will use this identifier to select pixels for which glacier melt must be computed *if module G1 is activated* (see Section 2.4). If modules G2 or G3 are selected, S3M v5.1 will use glacier thickness instead (see next paragraph).

Optionally, the user can also provide:

- a glacier-ID raster assigning specific pixels to a glacier according to an inventory;
- a glacier-thickness raster (in m);
- a debris-coefficient raster (see Equation 40);
- a Δh pivot table (see Section 2.6).

The glacier-ID raster expects each glacier to be indicated using an integer, and S3M v5.1 will initially compile a list of these unique integers as a glacier inventory for the simulation. If the Δh parametrization is chosen, then S3M expects one record of the pivot table for each of these integers. If any of these maps is not supplied, S3M v5.1 will initialize it on the fly using -9999 values, which is S3M's identifier for Not-a-Number values; note that this may lead to inconsistent or erroneous results. S3M v5.1 expects all static input rasters to be included in one single NetCDF file called Terrain_Data.nc.gz (Figure **??**). Some basic Python code to generate Terrain_Data.nc.gz is reported at and , including a JSON configuration file.

Content of Terrain_Data.nc.gz

Content of MeteoData_yyyymmddHHMM.nc.gz

Content of the NetCDF files expected by S3M v5.1 to ingest static and dynamic input data (related to topography and weather, respectively). Note the names of each field, which must be followed in order for S3M v5.1 to load the underlying data. Also note that these NetCDF files include grids with latitude and longitude as well as information regarding time and the reference system. Some Python code that can be adapted to generate these files is reported at . These images were obtained by opening example NetCDF files using Panoply (https://www.giss.nasa.gov/tools/panoply/)

5.0.1 Dynamic data

Content of Updating_yyyymmddHHMM.nc.gz

Content of SWEass_yyyymmddHHMM.nc.gz

Content of the NetCDF files expected by S3M v5.1 to ingest assimilation data. Note the names of each field, which must be strictly followed in order for S3M v5.1 to load the underlying data. Also note that these NetCDF files include grids with latitude and longitude as well as information regarding time and the reference system. These images were obtained by opening example NetCDF files using Panoply (https://www.giss.nasa.gov/tools/panoply/)

Mandatory weather input data include:

- air temperature;
- relative humidity;
- incoming shortwave radiation;
- total precipitation.

Weather data must be supplied as distributed raster files according to a common geographic grid and reference system, similar to static data. This geographic grid may in principle be different from the computational grid used by the model, as S3M v5.1 includes a regridding algorithm that automatically checks for concistency and resamples input data using a nearest-neighbor approach. Note, however, that this nearest-neighbor approach may be unsuitable for specific applications, as for example it does not conserve precipitation mass. The timestep of input data must be the same as the one chosen for model computations. If any of these weather-input maps is not supplied, S3M v5.1 will initialize it on the fly using -9999 values, which is S3M's identifier for Not-a-Number values; note that this may lead to inconsistent or erroneous results.

S3M v5.1 expects weather-input rasters for each time step to be included in one NetCDF file called MeteoData_yyyymmddHHMM.nc.gz, where yyyymmddHHMM must be replaced with the time-step year (four digits), month, day, hour, and minute (all two digits). Content of one of these files is showed in Figure **??**; note that wind fields are not necessary for S3M v5.1. Some code that can be adapted to prepare input files for S3M v5.1 using Python is available at .

5.0.1 Assimilation data

Assimilation data are supplied to S3M v5.1 in a similar format as weather data (Figure **??**): snow-depth and SCA are bundled in an Updating_yyyymmddHHMM.nc.gz NetCDF file, while SWE data are supplied in a SWEass_yyyymmddHHMM.nc.gz, where yyyymmddHHMM must be replaced with the time-step year (four digits), month, day, hour, and minute (all two digits). If assimilation is activated (see next paragraph), S3M v5.1 will look for each of these files every computational timestep; if any of these files is available for a given timestep, it will be loaded and ingested by the model, otherwise the model will throw a warning message and simply no assimilation for that time step will be performed. Some initial code that can be adapted to prepare these files for S3M v5.1 using Python is available at .

5.0.1 The Namelist

Besides input and assimilation data, a key step during run preparation is to set up a list of all model options, including paths, modules, and parameter values. In S3M v5.1, this list is referred to as a Namelist or Infofile and is supplied as an ordinary txt file in a pre-defined format. One example of Namelist is available at , while Table **??** details its entries, along with their format, meaning, and options. Further details on parameters and modules can be found in the main text (Section 2). Note that the name of each parameter in the Namelist may be different from notation used in Section 2, mainly because the Namelist reflects definitions used in the source code over the course of $\sim$15 years of model development. However, comments in the Namelist and details in Table **??** guarantees correspondence with Section 2.

5.1 Run execution

5.0.1 Compiling S3M

S3M v5.1 runs on Linux Debian/Ubuntu 64bit environments, and is expected to run with any other Linux system. On the other hand, no portability to Windows platform is currently possible. The model requires a number of libraries and packages to be pre-installed on the machine, such as the netcdf4 library to handle NetCDF files and a fortran compiler (gnu fortran or Intel fortran) to build the source code. Flood-PROOFS, CIMA Research Foundation's toolkit for hydrologic forecasting, offers a number of shell scripts to set up all required libraries (see) and to automatically compile S3M v5.1 (see). The user is strongly recommended to use these pre-existing shell scripts, as they automatically configure all required packages for running the model, perform a number of consistency checks, and allow one to pre-set executable name and properly link the netcdf4 library to model executable. The ReadMe file at explains this set-up phase step by step.

Once all libraries are installed and source code is compiled, S3M v5.1 is launched by storing in a given directory the executable (e.g., S3M_v5_p1.x file) and the Namelist (e.g., S3M_namelist.txt, see Section **??** and Table **??**). The user must then point to this directory through the command line and write:

```
$ ./S3M_v5_p1.x S3M_namelist.txt
```

Upon model initialization and throughout model execution, S3M v5.1 will return several pieces of information on the terminal, including as a minimum time-step data and warnings. Note that the user can increase the amount of information reported on the terminal by setting the debugging mode through the Namelist (see Table **??**).

5.0.1 The restart file

S3M v5.1 supports reading initial conditions from an external file and use those conditions to restart a simulation. This restart file is in NetCDF format and should include – as a minimum – rasters of SWE, SWE_D, SWE_W, snow age A_s, snow albedo, bulk-dry-snow density ρ_D, cumulative daily snowfall and melt, and average air temperature over the previous 1 and 10 days ($\bar{T}_{10d}$). If glacier modules G2 or G3 are activated, S3M will also look for glacier thickness and cumulative annual ice melt (only needed for G3), unless the user has instructed S3M to load glacier thickness from the static-data input file (Table **??**).

If any of these rasters is not available, S3M will set them to -9999 (missing values). If the restart option is not activated in the namelist (see Table **??**), then S3M will initialize them as appropriate. Because of its nature of forecasting model, the restart file in S3M is simply the relevant output file from a previous simulation; if so, an output file with timestamp 11PM is preferred as it is the most complete output file for that simulation day (see Section **??** for output-file format).

5.1 Run post-processing

Throughout model run, S3M saves NetCDF files with a number of select output variables. The frequency of these output files is chosen by the user through the Namelist (Table **??**). Similar to all input files, outputs come in the standard GNU-zip-compression format and are automatically generated with name S3M_yyyymmddHHMM.nc.gz, where yyyymmddHHMM is the time-step year (four digits), month, day, hour, and minute (all two digits).

Figure **??** shows the content of one of these output files, with Table **??** detailing the meaning of each field and how they relate to model variables in Section 2. Field names in the output files are occasionally different from notation used in Section 2, because S3M-output files are used by other models within CIMA's Flood-PROOFS toolkit and so naming strikes a balance across disciplinary jargon, model versions, and legacy with other tools. Note that the list in Figure **??** refers to the extended output mode as defined in the Namelist (Table **??**); Table **??** specifies which variables are also saved with a basic output mode.

S3M_201609012300.nc.gz	S3M_201609012300.nc.gz	Local File
AgeS	Snow Age	Geo2D
AlbedoS	Snow Albedo	Geo2D
H_S	Bulk Snow Depth	Geo2D
Latitude	Latitude Coordinate	2D
Longitude	Longitude Coordinate	2D
MeltingG	Glacier Melt	Geo2D
MeltingS	Snow Melt	Geo2D
MeltingSDayCum	Daily Cumulative Snow Melt	Geo2D
Outflow	Snowpack Runoff	Geo2D
Precip	Total Precipitation Amount	Geo2D
RainFall	Rainfall Amount	Geo2D
REff	Effective Rainfall	Geo2D
RefreezingS	Snow Refreezing	Geo2D
Rho_D	Dry Snow Density	Geo2D
RhoS	Bulk-Snow Density	Geo2D
RhoS0	Fresh-Snow Density	Geo2D
SnowFall	Snowfall Amount	Geo2D
SnowfallCum	Daily Cumulative Snowfall	Geo2D
SnowMask	Snow Mask	Geo2D
SWE	Snow Water Equivalent	Geo2D
SWE_D	Dry SWE	Geo2D
SWE_W	Wet SWE	Geo2D
T_10Days	Average T 10 Days	Geo2D
T_1Days	Air Temperature Last 1 Day	Geo2D
Theta_W	Bulk Vol. LWC	Geo2D
time	time definition of output datasets	—
times	times definition of output datasets	—

Content of the S3M NetCDF output file. This image was obtained by opening this NetCDF file using Panoply (https://www.giss.nasa.gov/too

[a] S3M v5.1 accepts assimilation and weather input data in binary format (integer or double) in addition to NetCDF. However, this is only allowed for legacy reasons and is discouraged for new applications, so we do not discuss the binary format in this paper. [b] See Section **??** for details on restarting a run. [c] If 0 is selected, then S3M will load glacier thickness from a restart file, which is useful when pausing and restarting multi-year simulations. [d] This must include the full path to the file between single quote marks, without the file name (e.g., '/home/S3M/'). [e] These data can either be stored in one folder, or preferably in a year/month/day directory. In the first case, one should specify here the full path of the folder between single quote marks (e.g., '/home/S3M/data/'). In the second case, one can use automatic directory construction through, e.g., '/home/S3M/data/$yyyy/$mm/$dd/'. [f] Comma separated. [g] Three comma-separated values. The four elevation bands are defined as (1) all pixels below first value in a1dAltRange; (2) all pixels between the second and the first values in a1dAltRange; (3) all pixels between the third and second values in a1dAltRange; (4) all pixels above the third value in a1dAltRange. [h] In previous, unpublished versions of S3M, this parameter was a multiplicative term in Equation 18 to compute a melting parameter for bare ice. This modification was supposed to account for albedo decay on ice, which is now an explicit variable in S3M (see Equation 15). While this parameter is still tunable in the current version of S3M, mainly for legacy reasons, it is recommended to set it to 1 for physical reasons. Accordingly, it was not included in Section 2. [i] The Kernel function in Equation 34 is set to 0 after this date and the assimilation-SWE map is discarded. [j] This parameter is an optional, multiplicative term in Equation 19 to reduce m_r in refreezing conditions, similar to Avanzi et al. (2015) or Schaefli et al. (2014). Owing to reasons discussed

in Section 2, it is recommended to set this parameter to 1. k Compared to m'_r, m'_{rad} cannot be inputed for elevation bands. This will be included in future releases. l Equation 40 is only applied for pixels where f_{debris} is larger than this threshold value.

Entries of S3M Namelist, their format, meaning, and options.

Entry Format Meaning Options

Entry Format Meaning Options

sDomainName String Domain name - iFlagDebugSet Integer Flag for debugging 0 (no) or 1 (yes) iFlagDebugLevel Integer Debugging verbosity 0 to 3 iFlagTypeData_Forcing_Gridded Integer MeteoData format 1 (bin int), 2 (bin dbl), 3 (NetCDF) iFlagTypeData_Updating_Gridded Integer Updating format 1 (bin int), 2 (bin dbl), 3 (NetCDF) iFlagTypeData_Ass_SWE_Gridded Integer Ass. SWE format 1 (bin int), 2 (bin dbl), 3 (NetCDF) iFlagRestart Integer Restarting a run 0 (no) or 1 (yes) iFlagSnowAssim Integer Assimilating Updating maps 0 (no) or 1 (yes) iFlagSnowAssim_SWE Integer Assimilating SWE maps 0 (no) or 1 (yes) iFlagIceMassBalance Integer Glacier module 0 (G1), 1 (G2), 2 (G3) iFlagThickFromTerrData Integer Loading glacier thickness from static data 0 (no) or 1 (yes) iFlagGlacierDebris Integer Glacier-debris correction (Eq. 40) 0 (no) or 1 (yes) iFlagOutputMode Integer Output-file format 0 (basic) or 1 (extended) iFlagAssOnlyPos Integer Assimilate only pos. differences 0 (no) or 1 (yes) a1dGeoForcing Real Comma-sep. MeteoData lower-left angle coordinate - a1dResForcing Real Comma-sep. MeteoData cell sizes - a1iDimsForcing Integer Comma-sep. MeteoData dimensions - iSimLength Integer Simulation length in hours - iDtModel Integer Model time-step in seconds - iDtData_Forcing Integer Model time-step in seconds - iDtData_Output Integer Output time-step in seconds - iDtData_Updating Integer Updating time-step in seconds - iDtData_AssSWE Integer Ass. SWE time-step in seconds - iScaleFactor_Forcing Integer MeteoData binary-data scaling factor - iScaleFactor_Update Integer Updating binary-data scaling factor - iScaleFactor_SWEass Integer Ass. SWE binary-data scaling factor - sTimeStart String Timestamp of simulation start - sTimeRestart String Timestamp of restart - sPathData_Static_Gridded String Path to static input data - sPathData_Forcing_Gridded String Path to weather input data - sPathData_Updating_Gridded String Path to Updating data - sPathData_Output_Gridded String Path to output data - sPathData_Restart_Gridded String Path to restart data - sPathData_SWE_Assimilation_Gridded String Path to Ass. SWE data - a1dArctUp Real Parameter m'_r for four elevation bands - a1dAltRange Real Elevation-band limits for parameter m'_r in m - iGlacierValue Integer Glacier identifier in glacier mask - dRhoSnowFresh Real Maximum fresh-snow density in kg m^{-3} - dRhoSnowMax Real Maximum bulk-snow density in kg m^{-3} - dRhoSnowMin Real Minimum bulk-snow density in kg m^{-3} - dSnowQualityThr Real Snow-quality threshold for assimilation - dMeltingTRef Real Threshold-temperature for melting (T_τ, in °C) - dIceMeltingCoeff Real Ice-melting coefficient Legacy param., see note and set to 1. iSWEassInfluence Integer Number of validity days after SWE-map issue date dWeightSWEass Real Maximum weight W in Equation 34. dRefreezingSc Real Optional multiplicative factor in Equation 19. See note and set to 1. dModFactorRadS Real Parameter m'_{rad} - sWYstart String Water-year starting month (two digits) - dDebrisThreshold Real Threshold-value in f_{debris} to apply Equation 40 - sCommandZipFile String Command to zip files - sCommandUnzipFile String Command to unzip files - sCommandRemoveFile String Command to remove files - dRhoW Real Liquid-water density in kg m^{-3} - sReleaseVersion String Model version - sAuthorNames String Authors - sReleaseDate String Release date -

a Equivalent precipitation is the sum of glacier melt and snowpack runoff (Avanzi et al., 2021). b Pixels with at least 0.1 mm of SWE (Section 2).

Output-file content (see Section **??** for details).

Entry Model variable Meaning Basic mode? Comments

Entry Model variable Meaning Basic mode? Comments

AgeS A_s Snow age Y - AlbedoS α_S Snow albedo Y - Cum_WY_MeltingG b_a Cum. annual mass balance Y Only with modules G2 and G3 H_S h_S Bulk-snow depth N - Ice_Thickness h_G Ice thickness Y Only with modules G2 and G3 Ice_Thickness_Change Δh_G Ice-thickness change Y Only with modules G2 and G3 MeltingG M_G Glacier melt N - MeltingS M Snow melt N - MeltingSDayCum - Cumulative daily snowmelt Y Only saved at 11PM Outflow O Snowpack runoff N - Precip P Total precipitation N - RainFall R_f Rainfall amount N - REff $O+M_G$ Equivalent precipitation Y - RefreezingS R Refreezing N - Rho_D ρ_D Dry bulk-snow density Y - RhoS ρ_S Bulk-snow density N - RhoS0 ρ_f Fresh-snow density N - SnowFall S_f Snowfall amount N - SnowfallCum - Cumulative daily snowfall Y Only saved at 11PM SnowMask - Snowmask Y - SWE_D SWE_D Dry Snow Water Equivalent Y - SWE_W SWE_W Wet Snow Water Equivalent Y - T_10Days $\bar{T}_{10d}$ Average 10-day temperature Y - T_1Days - Average 1-day temperature Y Only saved at 11PM Theta_W θ_W Bulk vol. liquid water content N -

References

Andreadis, K. M. and Lettenmaier, D. P.: Assimilating remotely sensed snow observations into a macroscale hydrology model, Advances in Water Resources, 29, 872 – 886, https://doi.org/https://doi.org/10.1016/j.advwatres.2005.08.004, 2006.

Anghileri, D., Voisin, N., Castelletti, A., Pianosi, F., Nijssen, B., and Lettenmaier, D. P.: Value of long-term streamflow forecasts to reservoir operations for water supply in snow-dominated river catchments, Water Resources Research, 52, 4209–4225, https://doi.org/10.1002/2015WR017864, 2016.

Avanzi, F., Yamaguchi, S., Hirashima, H., and De Michele, C.: Bulk volumetric liquid water content in a seasonal snowpack: modeling its dynamics in different climatic conditions, Advances in Water Resources, 86, 1 – 13, https://doi.org/10.1016/j.advwatres.2015.09.021, 2015.

Avanzi, F., De Michele, C., Morin, S., Carmagnola, C. M., Ghezzi, A., and Lejeune, Y.: Model complexity and data requirements in snow hydrology: seeking a balance in practical applications, Hydrological Processes, 2016.

Avanzi, F., Petrucci, G., Matzl, M., Schneebeli, M., and De Michele, C.: Early formation of preferential flow in a homogeneous snowpack observed by micro-CT, Water Resources Research, 53, 3713–3729, https://doi.org/10.1002/2016WR019502, https://agupubs.onlinelibrary.wiley.com/doi/abs/10.1002/2016WR019502, 2017.

Avanzi, F., Maurer, T., Malek, S., Glaser, S. D., Bales, R. C., and Conklin, M. H.: Feather River Hydrologic Observatory: Improving Hydrological Snowpack Forecasting for Hydropower Generation Using Intelligent Information Systems, Tech. rep., California's Fourth Climate Change Assessment, California Energy Commission, 2018.

Avanzi, F., Johnson, R. C., Oroza, C. A., Hirashima, H., Maurer, T., and Yamaguchi, S.: Insights Into Preferential Flow Snowpack Runoff Using Random Forest, Water Resources Research, 55, 10 727–10 746, https://doi.org/https://doi.org/10.1029/2019WR024828, https://agupubs.onlinelibrary.wiley.com/doi/abs/10.1029/2019WR024828, 2019.

Avanzi, F., Rungee, J., Maurer, T., Bales, R., Ma, Q., Glaser, S., and Conklin, M.: Climate elasticity of evapotranspiration shifts the water balance of Mediterranean climates during multi-year droughts, Hydrology and Earth System Sciences, 24, 4317–4337, https://doi.org/10.5194/hess-24-4317-2020, https://hess.copernicus.org/articles/24/4317/2020/, 2020.

Avanzi, F., Ercolani, G., Gabellani, S., Cremonese, E., Pogliotti, P., Filippa, G., Morra di Cella, U., Ratto, S., Stevenin, H., Cauduro, M., and Juglair, S.: Learning about precipitation lapse rates from snow course data improves water balance modeling, Hydrology and Earth System Sciences, 25, 2109–2131, https://doi.org/10.5194/hess-25-2109-2021, https://hess.copernicus.org/articles/25/2109/2021/, 2021.

Bales, R., Molotch, N. P., Painter, T. H., Dettinger, M. D., Rice, R., and Dozier, J.: Mountain hydrology of the western United States, Water Resources Research, 42, W08 432, https://doi.org/10.1029/2005WR004387, 2006.

Bales, R. C., Hopmans, J. W., O'Geen, A. T., Meadows, M., Hartsough, P. C., Kirchner, P., Hunsaker, C. T., and Beaudette, D.: Soil moisture response to snowmelt and rainfall in a Sierra Nevada mixed-conifer forest, Vadose Zone Journal, 10, 786–799, 2011.

Banfi, F. and De Michele, C.: A local model of snow-firn dynamics and application to Colle Gnifetti site, The Cryosphere Discussions, 2021, 1–32, https://doi.org/10.5194/tc-2020-357, https://tc.copernicus.org/preprints/tc-2020-357/, 2021.

Barnett, T. P., Adam, J. C., and Lettenmaier, D. P.: Potential impacts of a warming climate on water availability in snow-dominated regions, Nature, 438, 303–309, https://doi.org/10.1038/nature04141, 2005.

Barry, R. G.: The cryosphere – past, present, and future: a review of the frozen water resources of the world, Polar Geography, 34, 219–227, https://doi.org/10.1080/1088937X.2011.638146, https://doi.org/10.1080/1088937X.2011.638146, 2011.

Bartelt, P. and Lehning, M.: A physical SNOWPACK model for the Swiss avalanche warning Part I: numerical model, Cold Regions Science and Technology, 35, 123–145, https://doi.org/10.1016/S0165-232X(02)00074-5, 2002.

Bartolini, E., Allamano, P., Laio, F., and Claps, P.: Runoff regime estimation at high-elevation sites: a parsimonious water balance approach, Hydrology and Earth System Sciences, 15, 1661–1673, https://doi.org/10.5194/hess-15-1661-2011, 2011.

Beniston, M., Farinotti, D., Stoffel, M., Andreassen, L. M., Coppola, E., Eckert, N., Fantini, A., Giacona, F., Hauck, C., Huss, M., Huwald, H., Lehning, M., López-Moreno, J.-I., Magnusson, J., Marty, C., Morán-Tejéda, E., Morin, S., Naaim, M., Provenzale, A., Rabatel, A., Six, D., Stötter, J., Strasser, U., Terzago, S., and Vincent, C.: The European mountain cryosphere: a review of its current state, trends, and future challenges, The Cryosphere, 12, 759–794, https://doi.org/10.5194/tc-12-759-2018, https://tc.copernicus.org/articles/12/759/2018/, 2018.

Beven, K.: A manifesto for the equifinality thesis, Journal of Hydrology, 320, 18 – 36, https://doi.org/https://doi.org/10.1016/j.jhydrol.2005.07.007, http://www.sciencedirect.com/science/article/pii/S002216940500332X, the model parameter estimation experiment, 2006.

Blanchet, J., Marty, C., and Lehning, M.: Extreme value statistics of snowfall in the Swiss Alpine region, Water Resources Research, 45, W05 424, https://doi.org/10.1029/2009WR007916, 2009.

Blöschl, G.: Scaling issues in snow hydrology, Hydrological Processes, 13, 2149–2175, https://doi.org/10.1002/(SICI)1099-1085(199910)13:14/15<2149::AID-HYP847>3.0.CO;2-8, 1999.

Blöschl, G. and Sivapalan, M.: Scale issues in hydrological modelling: A review, Hydrological Processes, 9, 251–290, https://doi.org/10.1002/hyp.3360090305, 1995.

Bongio, M., Avanzi, F., and De Michele, C.: Hydroelectric power generation in an Alpine basin: future water-energy scenarios in a run-of-the-river plant, Advances in Water Resources, 94, 318 – 331, https://doi.org/https://doi.org/10.1016/j.advwatres.2016.05.017, 2016.

Boni, G., Castelli, F., Gabellani, S., Machiavello, G., and Rudari, R.: Assimilation of MODIS snow cover and real time snow depth point data in a snow dynamic model, in: 2010 IEEE International Geoscience and Remote Sensing Symposium, pp. 1788–1791, 2010.

Brock, B. W., Mihalcea, C., Kirkbride, M. P., Diolaiuti, G., Cutler, M. E. J., and Smiraglia, C.: Meteorology and surface energy fluxes in the 2005–2007 ablation seasons at the Miage debris-covered glacier, Mont Blanc Massif, Italian Alps, Journal of Geophysical Research: Atmospheres, 115, https://doi.org/https://doi.org/10.1029/2009JD013224, 2010.

Calonne, N., Geindreau, C., Flin, F., Morin, S., Lesaffre, B., Rolland du Roscoat, S., and Charrier, P.: 3-D image-based numerical computations of snow permeability: links to specific surface area, density, and microstructural anisotropy, The Cryosphere, 6, 939–951, https://doi.org/10.5194/tc-6-939-2012, http://www.the-cryosphere.net/6/939/2012/, 2012.

Carmagnola, C. M., Morin, S., Lafaysse, M., Domine, F., Lesaffre, B., Lejeune, Y., Picard, G., and Arnaud, L.: Implementation and evaluation of prognostic representations of the optical diameter of snow in the SURFEX/ISBA-Crocus detailed snowpack model, The Cryosphere, 8, 417–437, https://doi.org/10.5194/tc-8-417-2014, http://www.the-cryosphere.net/8/417/2014/, 2014.

Cluzet, B., Revuelto, J., Lafaysse, M., Tuzet, F., Cosme, E., Picard, G., Arnaud, L., and Dumont, M.: Towards the assimilation of satellite reflectance into semi-distributed ensemble snowpack simulations, Cold Regions Science and Technology, 170, 102 918, 2020.

Colbeck, S. C.: One-dimensional water flow through snow, Tech. rep., Cold Regions Research and Engineering Laboratory, Hanover, NH, USA, 1971.

Colbeck, S. C.: A theory of water percolation in snow, Journal of Glaciology, 11, 369–385, 1972.

Cuffey, K. M. and Paterson, W. S. B.: The physics of glaciers, Academic Press, 2010.

Cui, G., Bales, R., Rice, R., Anderson, M., Avanzi, F., Hartsough, P., and Conklin, M.: Detecting Rain–Snow-Transition Elevations in Mountain Basins Using Wireless Sensor Networks, Journal of Hydrometeorology, 21, 2061–2081, 2020.

Davaze, L., Rabatel, A., Arnaud, Y., Sirguey, P., Six, D., Letreguilly, A., and Dumont, M.: Monitoring glacier albedo as a proxy to derive summer and annual surface mass balances from optical remote-sensing data, The Cryosphere, 12, 271–286, https://doi.org/10.5194/tc-12-271-2018, https://www.the-cryosphere.net/12/271/2018/, 2018.

De Michele, C., Avanzi, F., Ghezzi, A., and Jommi, C.: Investigating the dynamics of bulk snow density in dry and wet conditions using a one-dimensional model, The Cryosphere, 7, 433–444, https://doi.org/10.5194/tc-7-433-2013, 2013.

DeWalle, D. R. and Rango, A.: Principles of Snow Hydrology, Cambridge University Press, 2011.

Diolaiuti, G., D'Agata, C., and Smiraglia, C.: Belvedere Glacier, Monte Rosa, Italian Alps: Tongue Thickness and Volume Variations in the Second Half of the 20th Century, Arctic, Antarctic, and Alpine Research, 35, 255–263, https://doi.org/10.1657/1523-0430(2003)035[0255:BGMRIA]2.0.CO;2, 2003.

Domine, F., Taillandier, A.-S., and Simpson, W. R.: A parameterization of the specific surface area of seasonal snow for field use and for models of snowpack evolution, Journal of Geophysical Research: Earth Surface, 112, n/a–n/a, https://doi.org/10.1029/2006JF000512, http://dx.doi.org/10.1029/2006JF000512, 2007.

Domine, F., Morin, S., Brun, E., Lafaysse, M., and Carmagnola, C. M.: Seasonal evolution of snow permeability under equi-temperature and temperature-gradient conditions, The Cryosphere, 7, 1915–1929, https://doi.org/10.5194/tc-7-1915-2013, http://www.the-cryosphere.net/7/1915/2013/, 2013.

Dozier, J., Bair, E. H., and Davis, R. E.: Estimating the spatial distribution of snow water equivalent in the world's mountains, Wiley Interdisciplinary Reviews: Water, 3, 461–474, https://doi.org/10.1002/wat2.1140, 2016.

Dramsch, J. S.: Chapter One - 70 years of machine learning in geoscience in review, in: Machine Learning in Geosciences, edited by Moseley, B. and Krischer, L., vol. 61 of *Advances in Geophysics*, pp. 1–55, Elsevier, https://doi.org/https://doi.org/10.1016/bs.agph.2020.08.002, https://www.sciencedirect.com/science/article/pii/S0065268720300054, 2020.

Dutra, E., Balsamo, G., Viterbo, P., Miranda, P. M. A., Beljaars, A., Schär, C., and Elder, K.: An Improved Snow Scheme for the ECMWF Land Surface Model: Description and Offline Validation, Journal of Hydrometeorology, 11, 899 – 916, https://doi.org/10.1175/2010JHM1249.1, https://journals.ametsoc.org/view/journals/hydr/11/4/2010jhm1249_1.xml, 2010.

Eiriksson, D., Whitson, M., Luce, C. H., Marshall, H. P., Bradford, J., Benner, S. G., Black, T., Hetrick, H., and McNamara, P.: An evaluation of the hydrologic relevance of lateral flow in snow at hillslope and catchment scales, Hydrological Processes, 27, 640–654, https://doi.org/10.1002/hyp.9666, 2013.

Endrizzi, S., Gruber, S., Dall'Amico, M., and Rigon, R.: GEOtop 2.0: simulating the combined energy and water balance at and below the land surface accounting for soil freezing, snow cover and terrain effects, Geoscientific Model Development, 7, 2831–2857, https://doi.org/10.5194/gmd-7-2831-2014, https://gmd.copernicus.org/articles/7/2831/2014/, 2014.

Essery, R.: A factorial snowpack model (FSM 1.0), Geoscientific Model Development, 8, 3867–3876, https://doi.org/10.5194/gmd-8-3867-2015, https://gmd.copernicus.org/articles/8/3867/2015/, 2015.

Fierz, C., Armstrong, R., Durand, Y., Etchevers, P., Greene, E., McClung, D., Nishimura, K., Satyawali, P., and Sokratov, S.: The International Classification for Seasonal Snow on the Ground, Tech. rep., IHP-VII Technical Documents in Hydrology N 83, IACS Contribution N 1, UNESCO - IHP, Paris, 2009.

Filippa, G., Maggioni, M., Zanini, E., and Freppaz, M.: Analysis of continuous snow temperature profiles from automatic weather stations in Aosta Valley (NW Italy): Uncertainties and applications, Cold Regions Science and Technology, 104 - 105, 54 – 62, 2014.

Flanner, M. G., Shell, K. M., Barlage, M., Perovich, D. K., and Tschudi, M. A.: Radiative forcing and albedo feedback from the Northern Hemisphere cryosphere between 1979 and 2008, Nature Geoscience, 4, 151–155, https://doi.org/10.1038/ngeo1062, 2011.

Follum, M. L., Downer, C. W., Niemann, J. D., Roylance, S. M., and Vuyovich, C. M.: A radiation-derived temperature-index snow routine for the GSSHA hydrologic model, Journal of Hydrology, 529, 723–736, https://doi.org/https://doi.org/10.1016/j.jhydrol.2015.08.044, https://www.sciencedirect.com/science/article/pii/S0022169415006599, 2015.

Forster, R. R., Box, J. E., van den Broeke, M. R., Miege, C., Burgess, E. W., van Angelen, J. H., Lenaerts, J. T. M., Koenig, L. S., Paden, J., Lewis, C., Prasad Gogineni, S., Leuschen, C., and McConnell, J. R.: Extensive liquid meltwater storage in firn within the Greenland ice sheet, Nature Geoscience, 7, 95–98, https://doi.org/10.1038/ngeo2043, 2014.

Froidurot, S., Zin, I., Hingray, B., and Gautheron, A.: Sensitivity of Precipitation Phase over the Swiss Alps to Different Meteorological Variables, Journal of Hydrometeorology, 15, 685–696, https://doi.org/10.1175/JHM-D-13-073.1, 2014.

Fyffe, C. L., Reid, T. D., Brock, B. W., Kirkbride, M. P., Diolaiuti, G., Smiraglia, C., and Diotri, F.: A distributed energy-balance melt model of an alpine debris-covered glacier, Journal of Glaciology, 60, 587–602, https://doi.org/10.3189/2014JoG13J148, 2014.

Gallet, J.-C., Domine, F., and Dumont, M.: Measuring the specific surface area of wet snow using 1310 nm reflectance, The Cryosphere, 8, 1139–1148, https://doi.org/10.5194/tc-8-1139-2014, http://www.the-cryosphere.net/8/1139/2014/, 2014.

Georgakakos, K. P., Graham, N. E., Carpenter, M., and Yao, H.: Integrating climate-hydrology forecasts and multi-objective reservoir management for northern California, Eos, Transactions American Geophysical Union, 86, 122–127, https://doi.org/10.1029/2005EO120002, 2004.

Ghanjkhanlo, H., Vafakhah, M., Zeinivand, H., and Fathzadeh, A.: Prediction of snow water equivalent using artificial neural network and adaptive neuro-fuzzy inference system with two sampling schemes in semi-arid region of Iran, Journal of Mountain Science, 17, 1712–1723, 2020.

Girons Lopez, M., Vis, M. J. P., Jenicek, M., Griessinger, N., and Seibert, J.: Assessing the degree of detail of temperature-based snow routines for runoff modelling in mountainous areas in central Europe, Hydrology and Earth System Sciences, 24, 4441–4461, https://doi.org/10.5194/hess-24-4441-2020, https://hess.copernicus.org/articles/24/4441/2020/, 2020.

Grossi, F., Lahaye, E., Moulins, A., Borroni, A., Rosso, M., and Tepsich, P.: Locating ship strike risk hotspots for fin whale (Balaenoptera physalus) and sperm whale (Physeter macrocephalus) along main shipping lanes in the North-Western Mediterranean Sea, Ocean Coastal Management, 212, 105 820, https://doi.org/https://doi.org/10.1016/j.ocecoaman.2021.105820, https://www.sciencedirect.com/science/article/pii/S0964569121003033, 2021.

Grünewald, T., Schirmer, M., Mott, R., and Lehning, M.: Spatial and temporal variability of snow depth and ablation rates in a small mountain catchment, The Cryosphere, 4, 215–225, https://doi.org/10.5194/tc-4-215-2010, 2010.

Guyomarc'h, G., Bellot, H., Vionnet, V., Naaim-Bouvet, F., Déliot, Y., Fontaine, F., Puglièse, P., Nishimura, K., Durand, Y., and Naaim, M.: A meteorological and blowing snow data set (2000–2016) from a high-elevation alpine site (Col du Lac Blanc, France, 2720 m a.s.l.), Earth System Science Data, 11, 57–69, https://doi.org/10.5194/essd-11-57-2019, https://essd.copernicus.org/articles/11/57/2019/, 2019.

Günther, D., Marke, T., Essery, R., and Strasser, U.: Uncertainties in Snowpack Simulations—Assessing the Impact of Model Structure, Parameter Choice, and Forcing Data Error on Point-Scale Energy Balance Snow Model Performance, Water Resources Research, 55, 2779–2800, https://doi.org/https://doi.org/10.1029/2018WR023403, https://agupubs.onlinelibrary.wiley.com/doi/abs/10.1029/2018WR023403, 2019.

Hanzer, F., Carmagnola, C. M., Ebner, P. P., Koch, F., Monti, F., Bavay, M., Bernhardt, M., Lafaysse, M., Lehning, M., Strasser, U., François, H., and Morin, S.: Simulation of snow management in Alpine ski resorts using three different snow models, Cold Regions Science and Technology, 172, 102 995, https://doi.org/https://doi.org/10.1016/j.coldregions.2020.102995, http://www.sciencedirect.com/science/article/pii/S0165232X19302034, 2020.

Harrison, B. and Bales, R.: Skill Assessment of Water Supply Forecasts for Western Sierra Nevada Watersheds, Journal of Hydrologic Engineering, 21, 04016 002, https://doi.org/10.1061/(ASCE)HE.1943-5584.0001327, 2016.

Heilig, A., Mitterer, C., Schmid, L., Wever, N., Schweizer, J., Marshall, H.-P., and Eisen, O.: Seasonal and diurnal cycles of liquid water in snow - measurements and modeling, Journal of Geophysical Research - Earth Surface, 2015.

Helbig, N., Moeser, D., Teich, M., Vincent, L., Lejeune, Y., Sicart, J.-E., and Monnet, J.-M.: Snow processes in mountain forests: interception modeling for coarse-scale applications, Hydrology and Earth System Sciences, 24, 2545–2560, https://doi.org/10.5194/hess-24-2545-2020, https://www.hydrol-earth-syst-sci.net/24/2545/2020/, 2020.

Hirashima, H., Avanzi, F., and Wever, N.: Wet-Snow Metamorphism Drives the Transition From Preferential to Matrix Flow in Snow, Geophysical Research Letters, 46, 14 548–14 557, https://doi.org/https://doi.org/10.1029/2019GL084152, https://agupubs.onlinelibrary.wiley.com/doi/abs/10.1029/2019GL084152, 2019.

Hock, R.: A distributed temperature-index ice- and snowmelt model including potential direct solar radiation, Journal of Glaciology, 45, 101–111, 1999.

Hock, R.: Temperature index melt modelling in mountain areas, Journal of Hydrology, 282, 104–115, 2003.

Huning, L. S. and AghaKouchak, A.: Global snow drought hot spots and characteristics, Proceedings of the National Academy of Sciences, 117, 19 753–19 759, https://doi.org/10.1073/pnas.1915921117, https://www.pnas.org/content/117/33/19753, 2020.

Huss, M. and Fischer, M.: Sensitivity of Very Small Glaciers in the Swiss Alps to Future Climate Change, Frontiers in Earth Science, 4, 34, https://doi.org/10.3389/feart.2016.00034, 2016.

Huss, M., Jouvet, G., Farinotti, D., and Bauder, A.: Future high-mountain hydrology: a new parameterization of glacier retreat, Hydrology and Earth System Sciences, 14, 815–829, https://doi.org/10.5194/hess-14-815-2010, https://www.hydrol-earth-syst-sci.net/14/815/2010/, 2010.

Immerzeel, W. W., van Beek, L. P. H., and Bierkens, M. F. P.: Climate Change Will Affect the Asian Water Towers, Science, 328, 1382–1385, 2010.

IPCC: Climate Change 2013: The Physical Science Basis. Contribution of Working Group I to the Fifth Assessment Report of the Intergovernmental Panel on Climate Change, Cambridge University Press, 2013.

IPCC: AR6 Climate Change 2021: The Physical Science Basis, 2021.

Jennings, K. S., Kittel, T. G. F., and Molotch, N. P.: Observations and simulations of the seasonal evolution of snowpack cold content and its relation to snowmelt and the snowpack energy budget, The Cryosphere, 12, 1595–1614, https://doi.org/10.5194/tc-12-1595-2018, https://www.the-cryosphere.net/12/1595/2018/, 2018.

Katsushima, T., Kumakura, T., and Takeuchi, Y.: A multiple snow layer model including a parameterization of vertical water channel process in snowpack, Cold Regions Science and Technology, 59, 143–151, https://doi.org/10.1016/j.coldregions.2009.09.002, 2009.

Katsushima, T., Yamaguchi, S., Kumakura, T., and Sato, A.: Experimental analysis of preferential flow in dry snowpack, Cold Regions Science and Technology, 85, 206–216, https://doi.org/10.1016/j.coldregions.2012.09.012, 2013.

Kelleners, T. J., Chandler, D. G., McNamara, J. P., Gribb, M. M., and Seyfried, M. S.: Modeling the Water and Energy Balance of Vegetated Areas with Snow Accumulation, Vadose Zone Journal, 8, 1013–1030, https://doi.org/10.2136/vzj2008.0183, 2009.

Kirchner, H. O. K., Michot, G., Narita, H., and Suzuki, T.: Snow as a foam of ice: plasticity, fracture and the brittle-to-ductile transition, Philosophical Magazine A, 81 (9), 2161–2181, 2001.

Kling, H., Fuchs, M., and Paulin, M.: Runoff conditions in the upper Danube basin under an ensemble of climate change scenarios, Journal of Hydrology, 424-425, 264 – 277, https://doi.org/https://doi.org/10.1016/j.jhydrol.2012.01.011, 2012.

Krol, Q. and Löwe, H.: Relating optical and microwave grain metrics of snow: the relevance of grain shape, The Cryosphere, 10, 2847–2863, https://doi.org/10.5194/tc-10-2847-2016, https://www.the-cryosphere.net/10/2847/2016/, 2016.

Lafaysse, M., Cluzet, B., Dumont, M., Lejeune, Y., Vionnet, V., and Morin, S.: A multiphysical ensemble system of numerical snow modelling, The Cryosphere, 11, 1173–1198, https://doi.org/10.5194/tc-11-1173-2017, https://tc.copernicus.org/articles/11/1173/2017/, 2017.

Laiolo, P., Gabellani, S., Rebora, N., Rudari, R., Ferraris, L., Ratto, S., Stevenin, H., and Cauduro, M.: Validation of the Flood-PROOFS probabilistic forecasting system, Hydrological Processes, 28, 3466–3481, https://doi.org/10.1002/hyp.9888, 2014.

Laramie, R. L. and Schaake, J. C. J.: Simulation of the continuous snowmelt process, Tech. rep., MIT, Cambridge, 1972.

Legagneux, L., Cabanes, A., and Dominé, F.: Measurement of the specific surface area of 176 snow samples using methane adsorption at 77 K, Journal of Geophysical Research: Atmospheres, 107, ACH 5–1–ACH 5–15, https://doi.org/10.1029/2001JD001016, http://dx.doi.org/10.1029/2001JD001016, 2002.

Lehning, M., Bartelt, P., Brown, B., and Fierz, C.: A physical SNOWPACK model for the Swiss avalanche warning Part III: meteorological forcing, thin layer formation and evaluation, Cold Regions Science and Technology, 35, 169–184, 2002.

Li, H., Beldring, S., Xu, C.-Y., Huss, M., Melvold, K., and Jain, S. K.: Integrating a glacier retreat model into a hydrological model – Case studies of three glacierised catchments in Norway and Himalayan region, Journal of Hydrology, 527, 656 – 667, https://doi.org/https://doi.org/10.1016/j.jhydrol.2015.05.017, http://www.sciencedirect.com/science/article/pii/S0022169415003674, 2015.

López Moreno, J. I., Fassnacht, S. R., Heath, J. T., Musselman, K. N., Revuelto, J., Latron, J., Móran-Tejeda, E., and Jonas, T.: Small scale spatial variability of snow density and depth over complex alpine terrain: Implications for estimating snow water equivalent, Advances in Water Resources, 55, 40–52, 2013.

Lundquist, J. D., Dickerson-Lange, S. E., Lutz, J. A., and Cristea, N. C.: Lower forest density enhances snow retention in regions with warmer winters: A global framework developed from plot-scale observations and modeling, Water Resources Research, 49, 6356–6370, https://doi.org/10.1002/wrcr.20504, 2013.

Machguth, H., MacFerrin, M., van As, D., Box, J. E., Charalampidis, C., Colgan, W., Fausto, R. S., Meijer, H. A. J., Mosley-Thompson, E., and van de Wal, R. S. W.: Greenland meltwater storage in firn limited by near-surface ice formation, Nature Climate Change, https://doi.org/10.1038/nclimate2899, 2016.

Magnusson, J., Wever, N., Essery, R., an A. Winstral, N. H., and Jonas, T.: Evaluating snow models with varying process representations for hydrological applications, Water Resources Research, 51, 2707 – 2723, 2015.

Marks, D., Kimball, J., Tingey, D., and Link, T.: The sensitivity of snowmelt processes to climate conditions and forest cover during rain-on-snow: a case study of the 1996 Pacific Northwest flood, Hydrological Processes, 12, 1269 – 1287, 1998.

Martinec, J.: Snowmelt-runoff model for stream flow forecasts, Nordic Hydrology, 6, 145–154, 1975.

Masiokas, M. H., Rabatel, A., Rivera, A., Ruiz, L., Pitte, P., Ceballos, J. L., Barcaza, G., Soruco, A., Bown, F., Berthier, E., Dussaillant, I., and MacDonell, S.: A Review of the Current State and Recent Changes of the Andean Cryosphere, Frontiers in Earth Science, 8, 99, https://doi.org/10.3389/feart.2020.00099, 2020.

Maurer, T., Avanzi, F., Oroza, C. A., Glaser, S. D., Conklin, M., and Bales, R. C.: Optimizing spatial distribution of watershed-scale hydrologic models using Gaussian Mixture Models, Environmental Modelling Software, 142, 105 076, https://doi.org/https://doi.org/10.1016/j.envsoft.2021.105076, https://www.sciencedirect.com/science/article/pii/S1364815221001195, 2021.

Mazzoleni, M., Noh, S. J., Lee, H., Liu, Y., Seo, D.-J., Amaranto, A., Alfonso, L., and Solomatine, D. P.: Real-time assimilation of streamflow observations into a hydrological routing model: effects of model structures and updating methods, Hydrological Sciences Journal, 63, 386–407, https://doi.org/10.1080/02626667.2018.1430898, https://doi.org/10.1080/02626667.2018.1430898, 2018.

Mitterer, C., Techel, F., Fierz, C., and Schweizer, J.: An operational supporting tool for assessing wet-snow avalanche danger, in: International Snow Science Workshop Grenoble - Chamonix Mont-Blanc - 2013, 2013.

Mizukami, N. and Perica, S.: Spatiotemporal Characteristics of Snowpack Density in the Mountainous Regions of the Western United States, Journal of Hydrometeorology, 9, 1416–1426, https://doi.org/http://dx.doi.org/10.1175/2008JHM981.1, 2008.

Morin, S., Domine, F., Dufour, A., Lejeune, Y., Lesaffre, B., Willemet, J.-M., Carmagnola, C., and Jacobi, H.-W.: Measurements and modeling of the vertical profile of specific surface area of an alpine snowpack, Advances in Water Resources, 55, 111 – 120, https://doi.org/http://dx.doi.org/10.1016/j.advwatres.2012.01.010, http://www.sciencedirect.com/science/article/pii/S0309170812000206, 2013.

Mosaffa, H., Sadeghi, M., Mallakpour, I., Naghdyzadegan Jahromi, M., and Pourghasemi, H. R.: Chapter 43 - Application of machine learning algorithms in hydrology, in: Computers in Earth and Environmental Sciences, edited by Pourghasemi, H. R., pp. 585–591, Elsevier, https://doi.org/https://doi.org/10.1016/B978-0-323-89861-4.00027-0, https://www.sciencedirect.com/science/article/pii/B9780323898614000270, 2022.

Mott, R., Scipión, D., Schneebeli, M., Dawes, N., and Lehning, M.: Orographic effects on snow deposition patterns in mountainous terrain, Journal of Geophysical Research, 119, 1419–1439, https://doi.org/10.1002/2013JD019880, 2014.

Nicholson, L. and Benn, D. I.: Calculating ice melt beneath a debris layer using meteorological data, Journal of Glaciology, 52, 463–470, https://doi.org/10.3189/172756506781828584, 2006.

Niwano, M., Aoki, T., Kuchiki, K., Hosaka, M., and Kodama, Y.: Snow Metamorphism and Albedo Process (SMAP) model for climate studies: Model validation using meteorological and snow impurity data measured at Sapporo, Japan, Journal of Geophysical Research: Earth Surface, 117, https://doi.org/https://doi.org/10.1029/2011JF002239, 2012.

Ohara, N. and Kavvas, M. L.: Field observations and numerical model experiments for the snowmelt process at a field site, Advances in Water Resources, 29, 194–211, https://doi.org/10.1016/j.advwatres.2005.03.016, 2006.

Pagano, T. C., Wood, A. W., Ramos, M.-H., Cloke, H. L., Pappenberger, F., Clark, M. P., Cranston, M., Kavetski, D., Mathevet, T., Sorooshian, S., and Verkade, J. S.: Challenges of Operational River Forecasting, Journal of Hydrometeorology, 15, 1692–1707, https://doi.org/10.1175/JHM-D-13-0188.1, 2014.

Paterson, W.: The Physics of Glaciers, Pergamon, 1994.

Pellicciotti, F., Brock, B., Strasser, U., Burlando, P., Funk, M., and Corripio, J.: An enhanced temperature-index glacier melt model including the shortwave radiation balance: development and testing for Haut Glacier d'Arolla, Switzerland, Journal of Glaciology, 51, 573–587, https://doi.org/10.3189/172756505781829124, 2005.

Piazzi, G., Thirel, G., Campo, L., and Gabellani, S.: A particle filter scheme for multivariate data assimilation into a point-scale snowpack model in an Alpine environment, The Cryosphere, 12, 2287–2306, https://doi.org/10.5194/tc-12-2287-2018, https://www.the-cryosphere.net/12/2287/2018/, 2018.

Pielmeier, C., Techel, F., Marty, C., and Stucki, T.: Wet snow avalanche activity in the Swiss Alps–trend analysis for mid-winter season, in: Proceedings of the International Snow Science Workshop, Grenoble and Chamonix, pp. 1240–1246, 2013.

Pinzer, B. R.: Dynamics of temperature gradient snow metamorphism, Ph.D. Dissertation, ETH Zurich, 2009.

Pomeroy, J. and Brun, E.: Physical properties of snow, Snow ecology: An interdisciplinary examination of snow-covered ecosystems, pp. 45–126, 2001.

Rango, A. and Martinec, J.: Revisiting the degree-day method for snowmelt computations, JAWRA Journal of the American Water Resources Association, 31, 657–669, 1995.

Rasmussen, R., Baker, B., Kochendorfer, J., Meyers, T., Landolt, S., Fischer, A. P., Black, J., Thériault, J. M., Kucera, P., Gochis, D., Smith, C., Nitu, R., Hall, M., Ikeda, K., and Gutmann, E.: How Well Are We Measuring Snow: The NOAA/FAA/NCAR Winter Precipitation Test Bed, Bulletin of the American Meteorological Society, 93, 811–829, https://doi.org/10.1175/BAMS-D-11-00052.1, 2012.

Razavi, S., Sheikholeslami, R., Gupta, H. V., and Haghnegahdar, A.: VARS-TOOL: A toolbox for comprehensive, efficient, and robust sensitivity and uncertainty analysis, Environmental Modelling Software, 112, 95–107, https://doi.org/https://doi.org/10.1016/j.envsoft.2018.10.005, https://www.sciencedirect.com/science/article/pii/S1364815218304766, 2019.

Revuelto, J., Billecocq, P., Tuzet, F., Cluzet, B., Lamare, M., Larue, F., and Dumont, M.: Random forests as a tool to understand the snow depth distribution and its evolution in mountain areas, Hydrological Processes, 34, 5384–5401, https://doi.org/https://doi.org/10.1002/hyp.13951, https://onlinelibrary.wiley.com/doi/abs/10.1002/hyp.13951, 2020.

Rigon, R., Bertoldi, G., and Over, T. M.: GEOtop: A Distributed Hydrological Model with Coupled Water and Energy Budgets, Journal of Hydrometeorology, 7, 371 – 388, https://doi.org/10.1175/JHM497.1, https://journals.ametsoc.org/view/journals/hydr/7/3/jhm497_1.xml, 2006.

Rössler, O., Froidevaux, P., Börst, U., Rickli, R., Martius, O., and Weingartner, R.: Retrospective analysis of a nonforecasted rain-on-snow flood in the Alps - a matter of model limitations or unpredictable nature?, Hydrology and Earth System Sciences, 18, 2265–2285, https://doi.org/10.5194/hess-18-2265-2014, 2014.

Rutter, N., Essery, R., Pomeroy, J., Altimir, N., Andreadis, K., Baker, I., Barr, A., Bartlett, P., Boone, A., Deng, H., Douville, H., Dutra, E., Elder, K., Ellis, C., Feng, X., Gelfan, A., Goodbody, A., Gusev, Y., Gustafsson, D., Hellström, R., Hirabayashi, Y., Hirota, T., Jonas, T., Koren, V., Kuragina, A., Lettenmaier, D., Li, W.-P., Luce, C., Martin, E., Nasonova, O., Pumpanen, J., Pyles, R. D., Samuelsson, P., Sandells, M., Schädler, G., Shmakin, A., Smirnova, T. G., Stähli, M., Stöckli, R., Strasser, U., Su, H., Suzuki, K., Takata, K., Tanaka, K., Thompson, E., Vesala, T., Viterbo, P., Wiltshire, A., Xia, K., Xue, Y., and Yamazaki, T.: Evaluation of forest snow processes models (SnowMIP2), Journal of Geophysical Research: Atmospheres, 114, https://doi.org/https://doi.org/10.1029/2008JD011063, 2009.

Ryan, W. A., Doesken, N. J., and Fassnacht, S. R.: Evaluation of Ultrasonic Snow Depth Sensors for U.S. Snow Measurements, Journal of Atmospheric and Oceanic Technology, 25, 667–684, https://doi.org/10.1175/2007JTECHA947.1, 2008.

Savenije, H. H. G.: The art of hydrology, Hydrology and Earth System Sciences, 13, 157–161, 2009.

Schaefli, B. and Huss, M.: Integrating point glacier mass balance observations into hydrologic model identification, Hydrology and Earth System Sciences, 15, 1227–1241, https://doi.org/10.5194/hess-15-1227-2011, https://www.hydrol-earth-syst-sci.net/15/1227/2011/, 2011.

Schaefli, B., Hingray, B., Niggli, M., and Musy, A.: A conceptual glacio-hydrological model for high mountainous catchments, Hydrology and Earth System Sciences, 9, 95–109, https://doi.org/10.5194/hess-9-95-2005, http://www.hydrol-earth-syst-sci.net/9/95/2005/, 2005.

Schaefli, B., Hingray, B., and Musy, A.: Climate change and hydropower production in the Swiss Alps: quantification of potential impacts and related modelling uncertainties, Hydrology and Earth System Sciences, 11, 1191–1205, https://doi.org/10.5194/hess-11-1191-2007, 2007.

Schaefli, B., Nicótina, L., Imfeld, C., Da Ronco, P., Bertuzzo, E., and Rinaldo, A.: SEHR-ECHO v1.0: a Spatially Explicit Hydrologic Response model for ecohydrologic applications, Geoscientific Model Development, 7, 2733–2746, https://doi.org/10.5194/gmd-7-2733-2014, https://www.geosci-model-dev.net/7/2733/2014/, 2014.

Seibert, J., Vis, M. J. P., Kohn, I., Weiler, M., and Stahl, K.: Technical note: Representing glacier geometry changes in a semi-distributed hydrological model, Hydrology and Earth System Sciences, 22, 2211–2224, https://doi.org/10.5194/hess-22-2211-2018, https://www.hydrol-earth-syst-sci.net/22/2211/2018/, 2018.

Serreze, M. C., Clark, M. P., Armstrong, R. L., McGinnis, D. A., and Pulwarty, R. S.: Characteristics of the western United States snowpack from snowpack telemetry (SNOTEL) data, Water Resources Research, 35, 2145–2160, https://doi.org/10.1029/1999WR900090, 1999.

Shen, C., Chen, X., and Laloy, E.: Editorial: Broadening the Use of Machine Learning in Hydrology, Frontiers in Water, 3, 38, https://doi.org/10.3389/frwa.2021.681023, https://www.frontiersin.org/article/10.3389/frwa.2021.681023, 2021.

Silvestro, F., Gabellani, S., Delogu, F., Rudari, R., and Boni, G.: Exploiting remote sensing land surface temperature in distributed hydrological modelling: the example of the Continuum model, Hydrology and Earth System Sciences, 17, 39–62, https://doi.org/10.5194/hess-17-39-2013, https://www.hydrol-earth-syst-sci.net/17/39/2013/, 2013.

Skiles, S. M., Mallia, D. V., Hallar, A. G., Lin, J. C., Lambert, A., Petersen, R., and Clark, S.: Implications of a shrinking Great Salt Lake for dust on snow deposition in the Wasatch Mountains, UT, as informed by a source to sink case study from the 13–14 April 2017 dust event, Environmental Research Letters, 13, 124 031, https://doi.org/10.1088/1748-9326/aaefd8, https://doi.org/10.1088/1748-9326/aaefd8, 2018.

Soruco, A., Vincent, C., Rabatel, A., Francou, B., Thibert, E., Sicart, J. E., and Condom, T.: Contribution of glacier runoff to water resources of La Paz city, Bolivia (16° S), Annals of Glaciology, 56, 147–154, https://doi.org/10.3189/2015AoG70A001, 2015.

Sturm, M., Goldstein, M. A., and Parr, C.: Water and life from snow: A trillion dollar science question, Water Resources Research, 53, 3534–3544, https://doi.org/https://doi.org/10.1002/2017WR020840, 2017.

Tarboton, D. G. and Luce, C. H.: Utah Energy Balance snow accumulation and melt model (UEB), Computer model technical description and users guide, Tech. rep., Utah Water Research Laboratory Utah State University and USDA Forest Service, 1996.

Techel, F. and Pielmeier, C.: Point observations of liquid water content in wet snow - investigating methodical, spatial and temporal aspects, The Cryosphere, 5, 405–418, https://doi.org/10.5194/tc-5-405-2011, http://www.the-cryosphere.net/5/405/2011/, 2011.

Terzago, S., Andreoli, V., Arduini, G., Balsamo, G., Campo, L., Cassardo, C., Cremonese, E., Dolia, D., Gabellani, S., von Hardenberg, J., Morra di Cella, U., Palazzi, E., Piazzi, G., Pogliotti, P., and Provenzale, A.: Sensitivity of snow models to the accuracy of meteorological forcings in mountain environment, Hydrology and Earth System Sciences Discussions, 2019, 1–32, https://doi.org/10.5194/hess-2019-511, https://www.hydrol-earth-syst-sci-discuss.net/hess-2019-511/, 2019.

Vionnet, V., Brun, E., Morin, S., Boone, A., Faroux, S., Le Moigne, P., Martin, E., and Willemet, J.-M.: The detailed snowpack scheme Crocus and its implementation in SURFEX v7.2, Geoscientific Model Development, 5, 773–791, https://doi.org/10.5194/gmd-5-773-2012, 2012.

Vionnet, V., Marsh, C. B., Menounos, B., Gascoin, S., Wayand, N. E., Shea, J., Mukherjee, K., and Pomeroy, J. W.: Multi-scale snowdrift-permitting modelling of mountain snowpack, The Cryosphere, 15, 743–769, https://doi.org/10.5194/tc-15-743-2021, https://tc.copernicus.org/articles/15/743/2021/, 2021.

Viviroli, D., Messerli, H. H. D. B., Meybeck, M., and Weingartner, R.: Mountains of the world, water towers for humanity: Typology, mapping, and global significance, Water Resources Research, 43, W07 447, 2007.

Wang, L., Zhou, J., Qi, J., Sun, L., Yang, K., Tian, L., Lin, Y., Liu, W., Shrestha, M., Xue, Y., Koike, T., Ma, Y., Li, X., Chen, Y., Chen, D., Piao, S., and Lu, H.: Development of a land surface model with coupled snow and frozen soil physics, Water Resources Research, 53, 5085–5103, https://doi.org/https://doi.org/10.1002/2017WR020451, 2017.

Webb, R. W., Jennings, K. S., Fend, M., and Molotch, N. P.: Combining Ground-Penetrating Radar With Terrestrial LiDAR Scanning to Estimate the Spatial Distribution of Liquid Water Content in Seasonal Snowpacks, Water Resources Research, 54, 10,339–10,349, https://doi.org/10.1029/2018WR022680, https://agupubs.onlinelibrary.wiley.com/doi/abs/10.1029/2018WR022680, 2018.

Wever, N., Fierz, C., Mitterer, C., Hirashima, H., and Lehning, M.: Solving Richards Equation for snow improves snowpack meltwater runoff estimations in detailed multi-layer snowpack model, The Cryosphere, 8, 257–274, https://doi.org/10.5194/tc-8-257-2014, http://www.the-cryosphere.net/8/257/2014/, 2014.

Wever, N., Vera Valero, C., and Fierz, C.: Assessing wet snow avalanche activity using detailed physics based snowpack simulations, Geophysical Research Letters, https://doi.org/10.1002/2016GL068428, 2016.

Würzer, S., Jonas, T., Wever, N., and Lehning, M.: Influence of initial snowpack properties on runoff formation during rain-on-snow events, Journal of Hydrometeorology, https://doi.org/http://dx.doi.org/10.1175/JHM-D-15-0181.1, 2016.

Würzer, S., Wever, N., Juras, R., Lehning, M., and Jonas, T.: Modelling liquid water transport in snow under rain-on-snow conditions – considering preferential flow, Hydrology and Earth System Sciences, 21, 1741–1756, https://doi.org/10.5194/hess-21-1741-2017, https://www.hydrol-earth-syst-sci.net/21/1741/2017/, 2017.

Zanotti, F., Endrizzi, S., Bertoldi, G., and Rigon, R.: The GEOTOP snow module, Hydrological Processes, 18, 3667–3679, https://doi.org/https://doi.org/10.1002/hyp.5794, https://onlinelibrary.wiley.com/doi/abs/10.1002/hyp.5794, 2004.

Zaramella, M., Borga, M., Zoccatelli, D., and Carturan, L.: TOPMELT 1.0: a topography-based distribution function approach to snowmelt simulation for hydrological modelling at basin scale, Geoscientific Model Development, 12, 5251–5265, https://doi.org/10.5194/gmd-12-5251-2019, https://gmd.copernicus.org/articles/12/5251/2019/, 2019.

Zheng, Z., Kirchner, P. B., and Bales, R. C.: Topographic and vegetation effects on snow accumulation in the southern Sierra Nevada: a statistical summary from lidar data, The Cryosphere, 10, 257–269, https://doi.org/10.5194/tc-10-257-2016, 2016.